

Non-BPS exact solutions and their relation to bions in $\mathbb{C}P^{N-1}$ models

Tatsuhiro Misumi*

Department of Mathematical Science, Akita University,

1-1 Tegata Gakuen-machi, Akita 010-8502, Japan

Research and Education Center for Natural Sciences, Keio University,

4-1-1 Hiyoshi, Yokohama, Kanagawa 223-8521, Japan

Muneto Nitta[†] and Norisuke Sakai[‡]

Department of Physics, and Research and Education Center for Natural Sciences,

Keio University, 4-1-1 Hiyoshi, Yokohama, Kanagawa 223-8521, Japan

We investigate non-BPS exact solutions in $\mathbb{C}P^{N-1}$ sigma models on $\mathbb{R}^1 \times S^1$ with twisted boundary conditions, by using the Din-Zakrzewski projection method. We focus on the relation of the non-BPS solutions to the ansatz of multi-instanton (bion) configurations and discuss their significance in the context of the resurgence theory. We find that the transition between seemingly distinct configurations of multi-instantons occur as moduli changes in the non-BPS solutions, and the simplest non-BPS exact solution corresponds to multi-bion configurations with fully-compressed double fractional instantons in the middle. It indicates that the non-BPS solutions make small but nonzero contribution to the resurgent trans-series as special cases of the multi-bion configurations. We observe a generic pattern of transitions between distinct multi-bion configurations (flipping partners), leading to the three essential properties of the non-BPS exact solution: (i) opposite sign for terms corresponding to the left and right infinities, (ii) symmetric location of fractional instantons, and (iii) the transition between distinct bion configurations. By studying the balance of forces, we show that the relative phases between the instanton constituents play decisive roles in stability and instability of the multi-instanton configurations. We discuss local and global instabilities of the solutions such as negative modes and the flow to the other saddle points, by considering the deformations of the non-BPS exact solutions within our multi-instanton ansatz. We also briefly discuss some classes of the non-BPS exact solutions in Grassmann sigma models.

*Electronic address: misumi(at)phys.akita-u.ac.jp

[†]Electronic address: nitta(at)phys-h.keio.ac.jp

[‡]Electronic address: norisuke.sakai(at)gmail.com

I. INTRODUCTION

Recent intensive study on the resurgence theory and the complexified path integral in quantum field theories and quantum mechanics has revealed the significance of topological soliton molecules, which are composed of (fractional) instantons and anti-instantons [1–34]. Imaginary ambiguities arising in amplitudes of topologically neutral configurations of composite solitons can cancel out those arising in non-Borel-summable perturbative series in certain quantum theories [7–16, 18–21, 23, 24, 35–37]. In particular, in field theories on compactified spacetime, these objects are termed as “bions” [7–10]. It is expected that a full semi-classical expansion in perturbative and non-perturbative sectors as bions, which is called a “resurgent” trans-series [38–64], leads to unambiguous and self-consistent definition of field theories in the same manner as the conjecture in quantum mechanics [65–72]. It is also discussed that the complexification of variables and parameters in path integrals play significant roles in the resurgence theory [29, 30].

In order to reach deeper understanding on bions and the related physics, it is of great importance to study examples in the field theory models in low-dimensions such as $\mathbb{C}P^{N-1}$ models [9, 10, 19–21, 23, 24], principal chiral models [13–15] and quantum mechanics [15–17, 21]. In particular, the $\mathbb{C}P^{N-1}$ model in 1+1 dimensions has been studied for a long time as a toy model of the Yang-Mills theory in 3+1 dimensions, because of similarities between them such as dynamical mass gap, asymptotic freedom and the existence of instantons. The $\mathbb{C}P^{N-1}$ model on $\mathbb{R}^1 \times S^1$ with \mathbb{Z}_N -twisted boundary conditions admits fractional instantons (domain-wall instantons) as Bogomol’nyi-Prasad-Sommerfield (BPS) solutions with the minimal topological charge ($Q = 1/N$) [73, 74] (see also Refs. [75]). A part of the nonperturbative contributions in resurgence theory comes from bion configurations, consisting of a fractional instanton and anti-instanton. They are most conveniently obtained by means of an ansatz which reduces to solutions of field equations asymptotically at large separations of constituent fractional (anti-)instantons [19–21, 24]. It has been found that the two-body forces change its character from attractive to repulsive as the relative phase of these fractional (anti-)instantons varies [19].

Non-BPS exact solutions in the $\mathbb{C}P^{N-1}$ model on $\mathbb{R}^1 \times S^1$ with a \mathbb{Z}_N -twisted boundary condition are found [11], by means of the Din-Zakrzewski projection method [76–78] generating a tower of non-BPS solutions from a BPS solution. The simplest non-BPS solution that they found corresponds to the configuration composed of one doubly-compressed fractional instanton ($Q = 2/N$) and two fractional anti-instantons ($Q = -1/N$) for $N \geq 3$. It is not yet clear how the balance of forces is achieved in the non-BPS exact solutions, in contrast to the naive configuration composed of the

double fractional instanton and two fractional anti-instantons, where the attractive force exists among the nearest constituents [19]. On the other hand, the non-BPS exact solutions have been known to have unstable directions (negative mode) [76]. However, the local and global instabilities such as negative modes and the flow to the other saddle points have not been explicitly worked out for the non-BPS exact solutions. It is also observed recently that the non-BPS exact solutions exhibit unexpected properties with respect to the clustering [18].

The purpose of this work is to investigate the properties of non-BPS exact solutions [11] by using the ansatz of multi-instanton configurations, which is used to obtain the nonperturbative contributions needed for the resurgence [19–21, 24]. We find that the non-BPS exact solutions are contained as subspaces of the parameter space of the ansatz, giving (a part of) the multi-instanton contributions, and hence they play a role in resurgence. Relative phases between constituent fractional instantons are found to play a decisive role to achieve the balance of forces. We also find that the transition between seemingly distinct configurations occurs as moduli parameters change in the non-BPS solutions, and the simplest non-BPS solution contains a multi-bion configuration with fully-compressed double fractional instantons. This fully-compressed double fractional instanton eliminates the strong phase dependence of two-body forces between a fractional instanton and anti-instanton [19], and helps to achieve the balance of forces in the non-BPS exact solution. We obtain a generic pattern of transitions among distinct multi-bion configurations (flipping partners), which helps to list various flipping partners in the non-BPS exact solutions. We observe the three essential properties of the non-BPS exact solutions : (i) opposite sign for terms corresponding to the left and right infinities, (ii) the symmetric location of instantons, and (iii) the transition between flipping partners. The balance of forces in the non-BPS exact solution is examined step by step, and many-body forces related to the relative phases are found to be important. We study the local and global instabilities of the non-BPS exact solution and find physical meaning of the negative modes and the flow to the other saddle points. We also briefly discuss some classes of the non-BPS exact solutions in Grassmann sigma models.

This paper is organized as follows. In Sec. II, we review the multi-bion ansatz and introduce the simplest non-BPS solution in the $\mathbb{C}P^{N-1}$ model on $\mathbb{R}^1 \times S^1$ with a \mathbb{Z}_N -twisted boundary condition. In Sec. III we discuss the transition between seemingly distinct configurations in the non-BPS solutions, and conjecture a generic structure of non-BPS solutions diagrammatically. In Sec. IV we show how the balance of force exists in the non-BPS solutions, and discuss essential properties of the solutions. In Sec. V we investigate local and global instabilities of the non-BPS solutions by deforming them within the multi-bion ansatz, and discuss the number of negative

modes. In Sec. VI we briefly discuss the simplest classes of non-BPS solutions in Grassmann sigma models. Section VII is devoted to a summary and discussion.

II. NON-BPS SOLUTIONS IN $\mathbb{C}P^{N-1}$ MODELS

A. The multi-instanton ansatz

Action density $s(x)$ and topological charge density $q(x)$ of the $\mathbb{C}P^{N-1}$ model in euclidean 2-dimensions are given in terms of a normalized row vector $n(x)$ of an N -component complex scalar fields $\omega(x)$ as

$$s(x) = \frac{1}{2\pi g^2} (D_\mu n)(D_\mu n)^\dagger = \frac{1}{2\pi g^2} (\partial_\mu n \partial_\mu n^\dagger + \partial_\mu n n^\dagger \partial_\mu n n^\dagger), \quad (1)$$

$$q(x) = \frac{-1}{2\pi} \epsilon_{\mu\nu} \partial_\mu A_\nu = \frac{-i}{2\pi} \epsilon_{\mu\nu} \partial_\mu (n \partial_\nu n^\dagger), \quad (2)$$

$$n(x) = \omega(x)/|\omega(x)|, \quad |\omega| = \sqrt{\omega \omega^\dagger}, \quad A_\mu = i n \partial_\mu n^\dagger. \quad (3)$$

The unnormalized vector field ω is also called a moduli matrix, since it contains entire informations of moduli for BPS solutions [79]. We denote the total action as S and the total topological charge as Q . The covariant derivative $D_\mu = \partial_\mu + iA_\mu$ is defined in terms of the composite gauge field A_μ . One should note that the unnormalized vector field $\omega(x)$ multiplied by arbitrary nonsingular functions should be identified, since it gives the same physical field $n(x)$. We compactify the x_2 direction as $x_2 + L \sim x_2$, and impose the \mathbb{Z}_N -twisted boundary conditions on n and ω

$$\omega(x_1, x_2 + L) = \Omega \omega(x_1, x_2), \quad \Omega = \text{diag.} \left[1, e^{2\pi i/N}, e^{4\pi i/N}, \dots, e^{2(N-1)\pi i/N} \right]. \quad (4)$$

The twisted boundary condition introduces effectively a potential which lifts the vacuum moduli of $\mathbb{C}P^{N-1}$ model, leaving only N discrete vacua : $n = (1, \dots, 0), \dots, (0, \dots, 1)$.

With $z = x_1 + ix_2, \bar{z} = x_1 - ix_2$, the holomorphic fields $\omega(z)$ solve the BPS equation $D_{\bar{z}} n = 0$, which automatically satisfies the field equation. The simplest BPS solution with the topological charge $Q = 1/N$ is the fractional instanton given by the following unnormalized N -component fields $\omega(x)$

$$\omega = (0, \dots, a e^{i\theta_a} e^{-\frac{2\pi}{NL} z}, 1, \dots, 0), \quad (5)$$

with moduli parameters $a \in \mathbb{R}$ and $-\pi < \theta \leq \pi$. One should note that the twisted boundary condition introduces the nontrivial x_1 dependence automatically, leading to the kink-like behavior

as follows. For $x_1 \ll 0$, the term $ae^{i\theta_a}e^{-\frac{2\pi}{NL}z}$ is dominant, while the term 1 is dominant for $x_1 \gg 0$. Whenever a single component dominates, the normalized vector n becomes a vacuum configuration as $(0, \dots, 1, \dots, 0)$. Consequently the action density $s(x)$ and topological charge density $q(x)$ are

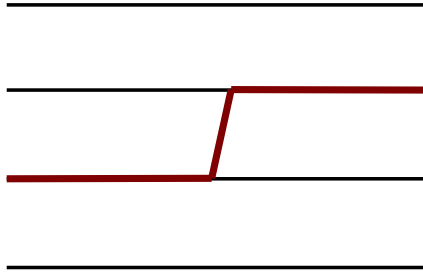


FIG. 1: An example of BPS fractional instantons in the \mathbb{CP}^{N-1} model. Black lines stand for some of N discrete vacua while a kinky red line indicates a transition between different vacua.

localized in a region of width NL around the transition point between the two vacua

$$\left(\dots, 1, 0, \dots \right) \rightarrow \left(\dots, 0, 1, \dots \right), \quad (6)$$

as depicted in Fig. 1. This kinky configuration has been understood as a D-brane configuration [80]. The condition $ae^{-\frac{2\pi}{NL}x_1} = 1$ gives the transition point at $x_1 = \frac{NL}{2\pi} \log a$, which is defined as the position of the fractional instanton. Because of the translational invariance, integrated total action does not depend on the position of the fractional instanton. Moreover, the action density $s(x)$ and topological charge density $q(x)$ do not depend on the phase angle θ_a .

It is important to note that both $s(x)$ and $q(x)$ for multi-fractional instantons ($|Q| < 1$) are independent of x_2 . Even if we have many fractional instantons at various locations, x_2 appears only as the phase factor $e^{-i\frac{2\pi}{NL}x_2}$ common to all terms in the same component due to the twisted boundary conditions (4). Then $s(x)$ and $q(x)$ do not depend on x_2 . In such a situation, we can take the compactification limit $L \rightarrow 0$, and obtain the domain wall situation that has been studied extensively [81, 82]. If and only if (more than) N fractional instantons coexist (not far apart), an additional term with a distinct x_2 dependent phase (by an additional amount $e^{-i\frac{2\pi}{L}x_2}$) coexists in the same component. In such a situation with $|Q| \geq 1$, x_2 dependence of $s(x)$ and $q(x)$ emerges.

From now on, we take the compactification scale $L = 1$ and the coupling constant $g^2 = 1$, for simplicity. Before discussing the non-BPS exact solutions in \mathbb{CP}^{N-1} models with the \mathbb{Z}_N -twisted boundary conditions (4), we introduce an ansatz [19, 23, 24] for multi fractional instanton

configurations that reduces to solutions of field equations for asymptotically large separations of constituent fractional instantons, and carries the correct number of moduli for each individual constituent: its phase and position in x_1 . Therefore the ansatz serves as a basis to obtain nonperturbative contributions by integrating over the (quasi)-moduli of the multi fractional instantons. Among them, we have bions (one-fractional-instanton + one-fractional-anti-instanton) that play a vital role to achieve a resurgent trans-series.

Let us first construct the ansatz for a bion as a non-BPS configuration as depicted in Fig. 2, by adding a fractional anti-instanton to the left of the fractional instanton (in Fig. 1). To return to the second vacuum for large negative x_1 , we need to add a term proportional to $e^{-\frac{2\pi}{N}(z+\bar{z})}$ in the second component in order to satisfy the twisted boundary condition (4). Thus the ansatz $\omega(x)$ for a bion in $\mathbb{C}P^{N-1}$ models is given by

$$\omega = (0, \dots, ae^{i\theta_a}e^{-\frac{2\pi}{N}z}, be^{i\theta_b}e^{-\frac{2\pi}{N}(z+\bar{z})} + 1, \dots, \dots, 0), \quad (7)$$

with $a, b \in \mathbb{R}$, $-\pi < \theta_a, \theta_b \leq \pi$. As x_1 varies from negative to positive values, the normalized vector n makes transitions between two different vacua as

$$(\dots, 0, 1, \dots) \rightarrow (\dots, 1, 0, \dots) \rightarrow (\dots, 0, 1, \dots). \quad (8)$$

The first transition point gives the position of the left fractional anti-instanton

$$x_{\bar{\mathcal{I}}} = \frac{N}{2\pi} \log \frac{b}{a}, \quad (9)$$

and the second transition point gives the position of the right fractional instanton

$$x_{\mathcal{I}} = \frac{N}{2\pi} \log a. \quad (10)$$

Thus, the separation R between these instanton constituents is

$$R = x_{\mathcal{I}} - x_{\bar{\mathcal{I}}} = \frac{N}{2\pi} \log \frac{a^2}{b}, \quad (11)$$

whereas the center of mass position is given by $x_{\text{cm}} = \frac{N}{4\pi} \log b$. The configuration associated with ω in Eq.(7) for $R > 1$ is depicted in Fig. 2.

We note that action density $s(x)$ and topological charge density $q(x)$ depend on the (relative) phase θ_b of two terms in a single component, but are independent of the phase θ_a . Because of translational invariance, the total energy is independent of the center of mass position x_{cm} . Therefore we consider densities $s(x)$ and $q(x)$ as functions of two relevant parameters : *the separation R between the fractional instanton and anti-instanton and the relative phase θ_b between them.* We

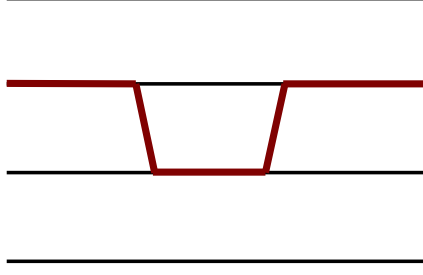


FIG. 2: An example of bion configurations in the \mathbb{CP}^{N-1} model. For simplicity, we depict only four vacua lines among N here.

also note that densities $s(x)$ and $q(x)$ of this configuration are independent of the coordinate x_2 of the compactified direction, since no instantons ($|Q| \geq 1$) is involved in any region of x_1 .

As shown in [19, 23, 24], by decreasing this separation R from positive to negative values, the value of the total action changes from $S = 2/N$ to $S = 0$. We can define the effective interaction potential between the two constituents as $V_{\text{eff}}(R, \theta_b) = S - S_{\mathcal{I}} - S_{\bar{\mathcal{I}}} = S - \frac{2}{N}$, representing the potential for the static two-body force between the constituent fractional instanton and fractional anti-instanton. For large separations R , we have found [19, 23, 24] that

$$V_{\text{eff}}(R, \theta_b) \propto -\cos \theta_b e^{-\xi R}, \quad \xi = 2\pi/N. \quad (12)$$

The notable point is that the interaction is attractive (repulsive) for $|\theta_b| \leq \pi/2$ ($\pi/2 \leq |\theta_b|$). Based on the extended Bogomolnyi–Zinn–Justin prescription [65, 66], it has been shown that the bion configuration in the \mathbb{CP}^{N-1} model produces the imaginary ambiguity [21], which is expected to cancel the imaginary ambiguity in the non-Borel-summable perturbative contributions similarly to the case in the quantum mechanics [65, 66].

Let us next introduce an ansatz for two bions. For simplicity, we assume $N \geq 3$ [87]. In order to add one more bion to the left of the single bion in Eq.(7) as in Fig. 3(a), we need to add a term $ce^{-\frac{2\pi}{N}(2z+\bar{z})}$ (with a complex constant c) in the first component, and another term $de^{-\frac{4\pi}{N}(z+\bar{z})}$ to the second component. We will call this diagram in Fig. 3(a) as $\bar{\mathcal{I}}\mathcal{I}\bar{\mathcal{I}}\mathcal{I}$. If we wish to consider the diagram with ordering $\bar{\mathcal{I}}\mathcal{I}\mathcal{I}\bar{\mathcal{I}}$ in Fig. 3(b), we need to have a term $fe^{-\frac{2\pi}{N}\bar{z}}$ in the third component. If we wish to consider the diagram with ordering $\mathcal{I}\bar{\mathcal{I}}\bar{\mathcal{I}}\mathcal{I}$ in Fig. 3(c), we need to have a term $ge^{-\frac{4\pi}{N}(z+2\bar{z})}$ in the third component. With these terms added, we obtain the ansatz for the most

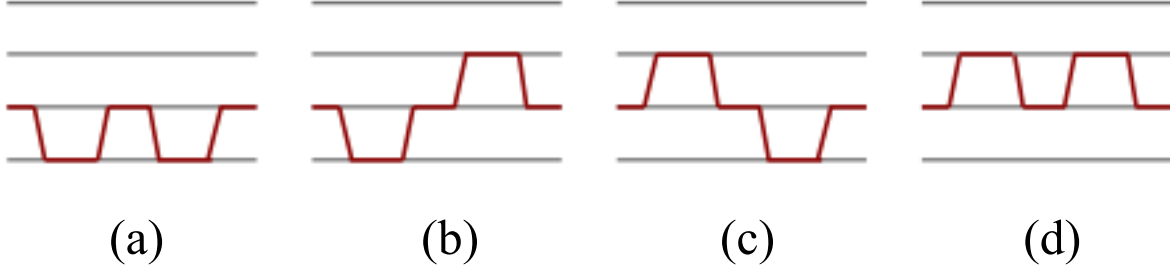


FIG. 3: Generic two-bion configurations in Eq. (13).

general configuration for two bions (with no (anti-)instanton with $|Q| = 1$ in any region of x_1)

$$\omega = \left(\dots, ae^{-\frac{2\pi}{N}z} + ce^{-\frac{2\pi}{N}(2z+\bar{z})}, 1 + be^{-\frac{2\pi}{N}(z+\bar{z})} + de^{-\frac{4\pi}{N}(z+\bar{z})}, fe^{-\frac{2\pi}{N}\bar{z}} + ge^{-\frac{2\pi}{N}(z+2\bar{z})}, \dots \right), \quad (13)$$

with seven complex parameters $a, b, c, d, f, g \in \mathbb{C}$. One should note that one more diagram with the ordering $\mathcal{I}\bar{\mathcal{I}}\mathcal{I}\bar{\mathcal{I}}$ in Fig. 3(d) is automatically included in the ansatz. The action and topological charge densities are independent of a phase common to terms in the same component. Therefore only four phases are relevant among six phase parameters : relative phases (a, c) , and (f, g) besides phases of b and d . Although six modulus correspond to six positions of constituent fractional (anti-)instantons, total action is independent of the center of mass position because of translational invariance. Therefore the action and topological charge densities can be considered as functions of only nine relevant parameters: four relative phases, five separation parameters corresponding to the lengths of bion and anti-bion, and the distance between them. This ansatz contains four seemingly-different configurations depending on the values of these parameters as shown in Fig. 3(a)-(d) for large separations.

Since our ansatz for the most general two-bion configurations in Eq. (13) does not have (anti-)instanton with $|Q| = 1$, all terms in the same component have a common x_2 -dependence as a phase factor such as $e^{-i\frac{2\pi}{N}x_2}$. Therefore the action density $s(x)$ and the topological charge density $q(x)$ are independent of x_2 in our ansatz. If (anti-)instanton with $|Q| = 1$ would be involved, additional terms with distinct x_2 -dependent phase factor would emerge such as $C(x_1)e^{-(2\pi/N)ix_2} + C'(x_1)e^{-(2\pi/N+2\pi)ix_2}$, and $s(x), q(x)$ would depend on x_2 .

Let us first consider the case with $|g| \gg |c|$ and $|a| \gg |f|$, where the terms with c and f are superficially negligible. Then, as x_1 varies from negative infinity to positive infinity, the dominant

term changes as $de^{-\frac{4\pi}{N}(z+\bar{z})} \rightarrow ge^{-\frac{2\pi}{N}(z+2\bar{z})} \rightarrow be^{-\frac{2\pi}{N}(z+\bar{z})} \rightarrow ae^{-\frac{2\pi}{N}z} \rightarrow 1$ for a choice of the parameters $|g|^2 \gg |b||d|$, $|b|^2 \gg |a||g|$, $|a|^2 \gg |b|$. It means that the vacua undergo the transition

$$(0, 1, 0) \rightarrow (0, 0, 1) \rightarrow (0, 1, 0) \rightarrow (1, 0, 0) \rightarrow (0, 1, 0), \quad (14)$$

as shown in Fig. 3(c). Using a similar reasoning as the bion case, we find the four fractional instanton constituents show up successively as x_1 increases from negative infinity to positive infinity : the first fractional instanton at $R_1 = \frac{N}{2\pi} \log \frac{|d|}{|g|}$, the first fractional anti-instanton at $R_2 = \frac{N}{2\pi} \log \frac{|g|}{|b|}$, the second fractional anti-instanton at $R_3 = \frac{N}{2\pi} \log \frac{|b|}{|a|}$, and the second fractional instanton at $R_4 = \frac{N}{2\pi} \log |a|$. The three separations between these instanton constituents are

$$R_{21} = \frac{N}{2\pi} \log \frac{|g|^2}{|b||d|}, \quad R_{32} = \frac{N}{2\pi} \log \frac{|b|^2}{|a||g|}, \quad R_{43} = \frac{N}{2\pi} \log \frac{|a|^2}{|b|}. \quad (15)$$

The configuration in Fig. 3(c) is visible in the parameter region $|d/g| \ll |g/b| \ll |b/a| \ll |a|$.

On the other hand, we can recognize the configuration in Fig. 3(b) in another region of the parameter space: the case with $|c| \gg |g|$ and $|f| \gg |a|$, where the terms with g and a are superficially negligible. Then we obtain transitions of vacua as

$$(0, 1, 0) \rightarrow (1, 0, 0) \rightarrow (0, 1, 0) \rightarrow (0, 0, 1) \rightarrow (0, 1, 0), \quad (16)$$

instead of Eq. (14). As x_1 increases from negative infinity to positive infinity, four fractional instanton constituents show up successively : the first fractional anti-instanton at $R'_1 = \frac{N}{2\pi} \log \frac{|d|}{|c|}$, the first fractional instanton at $R'_2 = \frac{N}{2\pi} \log \frac{|c|}{|b|}$, the second fractional instanton at $R'_3 = \frac{N}{2\pi} \log \frac{|b|}{|f|}$, and the second fractional anti-instanton at $R'_4 = \frac{N}{2\pi} \log |f|$. Thus, the three separations between these instanton constituents are

$$R'_{21} = \frac{N}{2\pi} \log \frac{|c|^2}{|b||d|}, \quad R'_{32} = \frac{N}{2\pi} \log \frac{|b|^2}{|c||f|}, \quad R'_{43} = \frac{N}{2\pi} \log \frac{|f|^2}{|b|}. \quad (17)$$

The configuration in Fig. 3(b) is visible in the parameter region $|d/c| \ll |c/b| \ll |b/f| \ll |f|$. We note that there is a relation among six separations $R_{21} + 2R_{32} + R_{43} = R'_{21} + 2R'_{32} + R'_{43}$, leading to five independent separation variables. In both of these parameter regions corresponding to Fig. 3(b) and (c), only two phases of b and d are relevant, since only a single term is dominant in the first and the third components.

It is interesting to note that the most general ansatz for two bions automatically contains two other possible diagrams containing the ordering $\bar{I}I\bar{I}I$ in Fig. 3(a), or $I\bar{I}I\bar{I}$ in Fig. 3(d). The configuration of $\bar{I}I\bar{I}I$ in Fig. 3(a) is visible in the parameter region $|d/c| \ll |c/b| \ll |b/a| \ll |a|$. In this parameter region, the relative phases (a, c) , and phases of b and d are relevant among the

four phase parameters. The configuration of $\mathcal{I}\bar{\mathcal{I}}\mathcal{I}\bar{\mathcal{I}}$ in Fig. 3(d) is visible in the parameter region $|d/g| \ll |g/b| \ll |b/f| \ll |f|$, where only three phases are relevant : the relative phase (g, f) and phases b and d . It is interesting to note that a different partial set of four relative phases are relevant in each parameter region corresponding to four different diagrams in Fig. 3. One should also note that there are five independent length parameters, but only three different combinations of them emerge as separations of constituent fractional (anti-)instantons in different parameter regions. In the next section, we will demonstrate that this ansatz (13) contains the simplest non-BPS exact solution. This fact implies that the non-BPS exact solution contributes to the resurgent expansion as a special configuration of two-bion configurations.

B. The simplest non-BPS exact solution

Based on the procedure of projection operations [76], the non-BPS exact solutions in $\mathbb{C}P^{N-1}$ model on $\mathbb{R}^1 \times S^1$ with \mathbb{Z}_N -twisted boundary conditions are constructed in [11]. We here discuss the properties of the solutions. The non-BPS solutions are obtained through the following projection applied to any of the BPS solutions ω ,

$$Z_+ : \omega \rightarrow Z_+\omega \equiv \partial_z \omega - \frac{(\partial_z \omega) \omega^\dagger}{\omega \omega^\dagger} \omega. \quad (18)$$

Starting from the BPS solution of two fractional instantons in $\mathbb{C}P^2$ model with \mathbb{Z}_N -twisted bound-

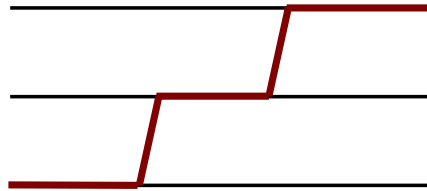


FIG. 4: BPS solution $\omega_{\mathcal{I}\mathcal{I}}$ of two fractional instantons in Eq. (19) in $\mathbb{C}P^2$ model.

ary condition

$$\omega_{\mathcal{I}\mathcal{I}} = \left(l_1 e^{i\theta_1} e^{-\frac{4\pi}{3}z}, l_2 e^{i\theta_2} e^{-\frac{2\pi}{3}z}, 1 \right), \quad (19)$$

with $S = 2/3$, $Q = 2/3$ shown in Fig. 4, the projection produces the non-BPS exact solution

$$\omega_{\text{nbp}} = \left(e^{i\theta_1} \left(\frac{2l_1}{l_2} e^{-\frac{2\pi}{3}z} + l_1 l_2 e^{-\frac{2\pi}{3}(2z+\bar{z})} \right), e^{i\theta_2} \left(1 - l_1^2 e^{-\frac{4\pi}{3}(z+\bar{z})} \right), -l_2 e^{-\frac{2\pi}{3}\bar{z}} - \frac{2l_1^2}{l_2} e^{-\frac{2\pi}{3}(z+2\bar{z})} \right). \quad (20)$$

The total action of this solution is $S = 4/3$ while the total topological charge is $Q = 0$. This ω is obviously a special case of the generic two-bion configuration (13). We note that the action $s(x)$ and topological $q(x)$ charge densities are independent of overall phase variables θ_1, θ_2 in each component.

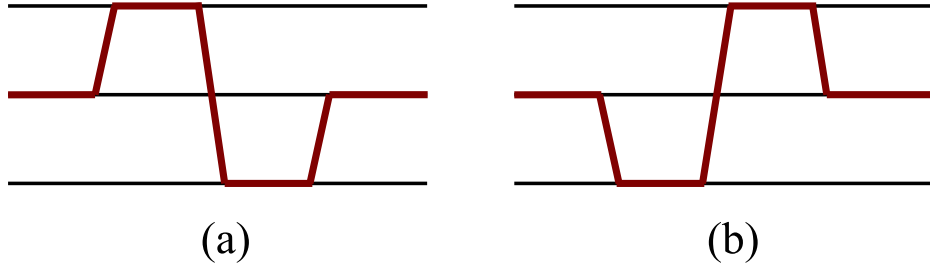


FIG. 5: The non-BPS exact solution in \mathbb{CP}^2 model makes transition between these two configurations (flipping partners) as a moduli $2l_1/l_2^2$ varies.

The exact solution (20) is included as a subspace of parameters in our most general ansatz in Eq. (13) as :

$$a = 2l_1/l_2, \quad c = l_1 l_2, \quad b = 0, \quad d = -l_1^2, \quad f = -l_2, \quad g = -2l_1^2/l_2. \quad (21)$$

What is special in this solution is that this solution contains in different corners of moduli space the two seemingly distinct configurations, each of which can be seen as a compressed case of the *two fractional (anti-)instanton configuration* in the middle, because of $b = 0$. As depicted in Fig. 5, the solution can describe two types of configurations depending on the ratio of $2l_1$ and l_2^2 : Fig. 5(a) arises for $2l_1 \gg l_2^2$, and contains locally one compressed double fractional anti-instanton sandwiched between two fractional instantons, whereas Fig. 5(b) arises for $2l_1 \ll l_2^2$, and contains locally one compressed double fractional instanton sandwiched between two fractional anti-instantons and one double fractional instanton. These two configurations are similar to the two-bion configuration in Fig. 3(c) and (b), but the two adjacent fractional (anti-)instantons are completely compressed. Let us call these two configurations as the flipping partners. We show how densities of action $s(x)$

and topological charge $q(x)$ vary as $2l_1/l_2^2$ varies in Fig. 6, although the value of the integrated total action remains constant. We find the action densities of flipping partners are related by the transformation $l_2/\sqrt{2} \rightarrow \sqrt{2}/l_2$.

We will find that the flipping partners contained in the non-BPS exact solution is important to achieve the balance of forces between the BPS and anti-BPS constituent fractional instantons. One should also note that the two separations R_1 (R'_1) and R_2 (R'_2) from the middle compressed fractional instantons to the left and right fractional instantons are identical :

$$R_1 = R_2 = \frac{3}{4\pi} \log(4l_1/l_2^2), \quad (22)$$

for $2l_1 \gg l_2^2$ and

$$R'_1 = R'_2 = \frac{3}{4\pi} \log(l_2^2/l_1), \quad (23)$$

for $2l_1 \ll l_2^2$.

III. FLIPPING PARTNERS AND GENERIC CONSTRUCTION

A. Flipping partners in the non-BPS exact solution

Let us analyze how transitions between different configurations occur in the non-BPS exact solution in the \mathbb{CP}^2 model as shown in Fig. 5 (the extension to \mathbb{CP}^{N-1} models is straightforward). We can re-express the BPS solution with two fractional-instantons in Eq.(19) as

$$\begin{aligned} \omega_{II} &= \left(A(z), \quad B(z), \quad 1 \right), \\ A(z) &= l_1 e^{i\theta_1} e^{-2\alpha z}, \quad B(z) = l_2 e^{i\theta_2} e^{-\alpha z}, \end{aligned} \quad (24)$$

with $\alpha = 2\pi/3$. Then, the projection operation in Rq.(18) gives a non-BPS exact solution in Eq.(20), which is now re-expressed as

$$\omega_{\text{nbps}} = \left(A(B\bar{B} + 2) \quad B(-A\bar{A} + 1) \quad 2A\bar{A} + B\bar{B} \right), \quad (25)$$

where the difference by an overall factor from Eq.(20) is irrelevant.

We now explain how various constituents emerge in the non-BPS exact solution : (a)fractional anti-instantons, (b)fractional instantons, (c)double fractional instantons, and (d)double fractional anti-instantons.

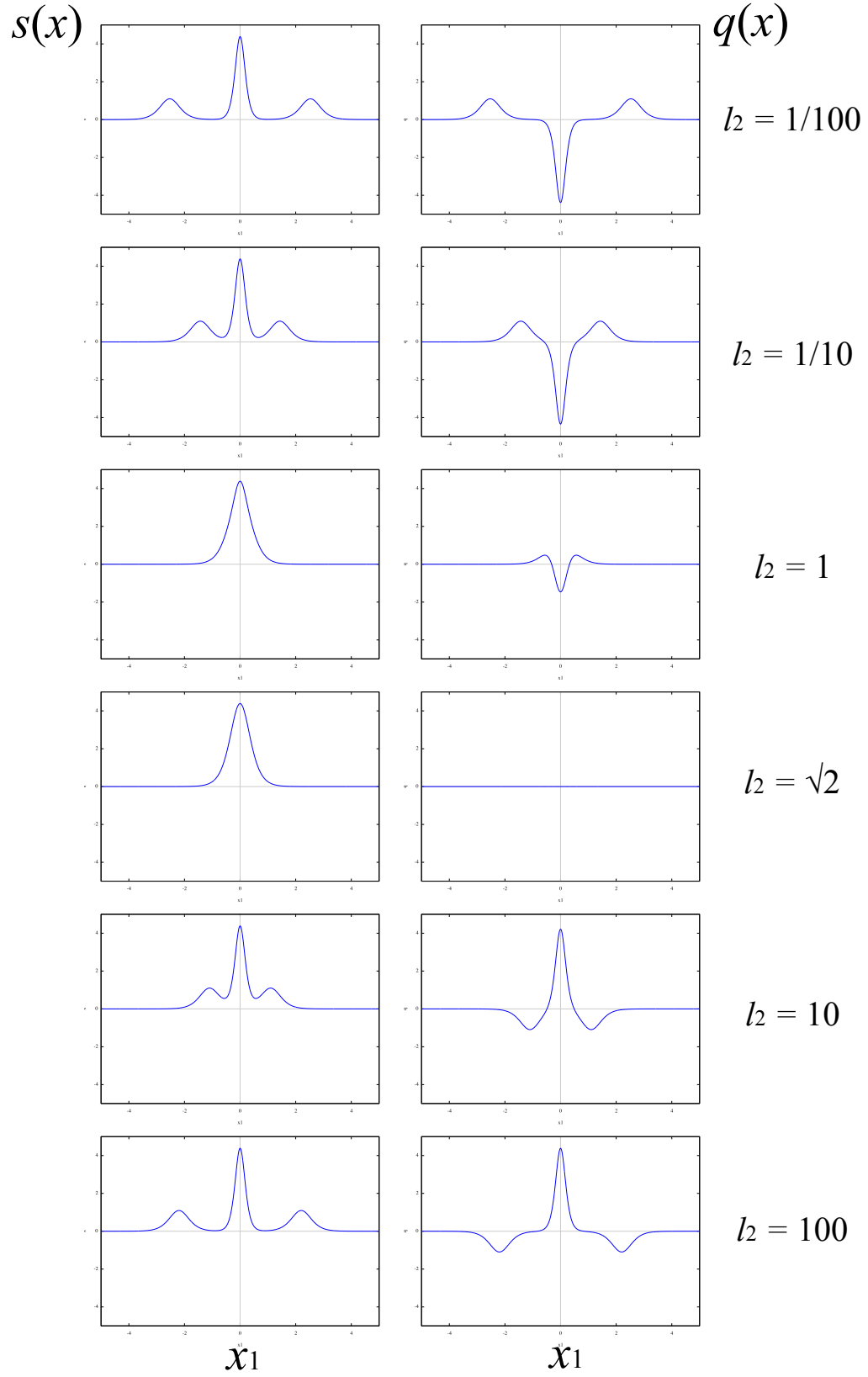


FIG. 6: Action density $s(x)$ (left) and topological charge density $q(x)$ (right) of the non-BPS solution Eq.(20) with $l_2 = 1/100, 1/10, 1, \sqrt{2}, 10, 100$ (from top to bottom) with $l_1 = 1$ fixed.

(a) Fractional anti-instantons

When $AB\bar{B}$ in the first component and $-BA\bar{A}$ in the second component are dominant, the unnormalized vector field ω is equivalent to a simpler one as

$$\omega_{\text{nbps}} \approx \begin{pmatrix} AB\bar{B} & -BA\bar{A} & 0 \end{pmatrix} \sim \begin{pmatrix} \bar{B}, & -\bar{A}, & 0 \end{pmatrix}, \quad (26)$$

because the division of ω by a common factor AB to all components gives identical physical vector n . Since $|\bar{B}| = l_2 e^{-\alpha x_1}$ and $|\bar{A}| = l_1 e^{-2\alpha x_1}$, the vacua undergo transition as $(0, 1, 0) \rightarrow (1, 0, 0)$, implying a fractional anti-instanton at $x_1 = (1/\alpha) \log(l_1/l_2)$. In the same manner, when B in the second component and $B\bar{B}$ in the third component are dominant, we obtain

$$\omega_{\text{nbps}} \approx \begin{pmatrix} 0, & B, & B\bar{B} \end{pmatrix} \sim \begin{pmatrix} 0, & 1, & \bar{B} \end{pmatrix}, \quad (27)$$

which implies the vacuum transition $(0, 0, 1) \rightarrow (0, 1, 0)$ and a fractional anti-instanton at $x_1 = (1/\alpha) \log l_2$. These two fractional anti-instantons correspond to upside-down constituents (instanton \rightarrow anti-instanton) of the original BPS solution in Fig. 4.

(b) Fractional instantons

When $2A$ in the first component and B in the second component are dominant, we obtain

$$\omega_{\text{nbps}} \approx \begin{pmatrix} 2A, & B, & 0 \end{pmatrix}, \quad (28)$$

which implies the vacuum transition $(1, 0, 0) \rightarrow (0, 1, 0)$ and a fractional instanton at $x_1 = (1/\alpha) \log(2l_1/l_2)$. When $-BA\bar{A}$ in the second component and $2A\bar{A}$ in the third component are dominant, we obtain

$$\omega_{\text{nbps}} \approx \begin{pmatrix} 0, & -BA\bar{A}, & 2A\bar{A} \end{pmatrix} \sim \begin{pmatrix} 0, & -B, & 2 \end{pmatrix}, \quad (29)$$

implying the vacuum transition $(0, 1, 0) \rightarrow (0, 0, 1)$ and a fractional instanton at $x_1 = (1/\alpha) \log(l_2/2)$. These two fractional instantons correspond to the constituents of the original BPS solution in Fig. 4.

(c) Double fractional instantons

When $AB\bar{B}$ in the first component and $B\bar{B}$ in the third component are dominant, we obtain

$$\omega_{\text{nbps}} \approx \begin{pmatrix} AB\bar{B}, & 0, & B\bar{B} \end{pmatrix} \sim \begin{pmatrix} A, & 0, & 1 \end{pmatrix}, \quad (30)$$

implying the vacuum transition $(1, 0, 0) \rightarrow (0, 0, 1)$ and a compressed double fractional instanton at $x_1 = (1/(2\alpha)) \log l_1$.

(d) Double fractional anti-instantons

When $2A$ in the first component and $2A\bar{A}$ in the third component re dominant, we obtain

$$\omega_{\text{nbps}} \approx \left(2A, \ 0, \ 2A\bar{A} \right) \sim \left(1, \ 0, \ \bar{A} \right). \quad (31)$$

implying the vacuum transition $(0,0,1) \rightarrow (1,0,0)$, and a compressed double fractional anti-instanton at $x_1 = (1/(2\alpha)) \log l_1$.

If $2l_1 > l_2^2$, the conditions for (b) and (d) are satisfied and the configuration in Fig. 5(a) is clearly visible. On the other hand, the conditions for (a) and (c) are satisfied and the configuration in Fig. 5(b) is visible if $2l_1 < l_2^2$.

We also note that the left and right fractional anti-instantons in (b) can be regarded as upside-down of fractional instantons in the original BPS solution in Fig. 4. The configuration in (a) can be obtained by reflecting (b) in the middle. These observations leads to a generic pattern of non-BPS exact solutions constructed from the BPS-solutions and to a graphical construction of various configurations contained in the non-BPS exact solution in the next subsection.

B. Generic pattern of non-BPS exact solutions

We have seen how two different configurations emerge in a single non-BPS exact solution as moduli varies. Since this feature is quite generic in non-BPS exact solutions, we now summarize our observation on generic patterns of various configurations contained in non-BPS exact solutions. Below, we begin with the original BPS solution and show how various configurations in the non-BPS exact solution can be graphically obtained :

1. Turn all the BPS constituents upside down in the original BPS solution (fractional instanton \leftrightarrow fractional anti-instanton).
2. Connect the constituents by multiple instantons (double fractional instanton, triple fractional instanton etc.). Then we end up with one of configurations of the non-BPS solution.
3. Non-BPS solutions also contain configurations, in which the part with zero-instanton number is reflected in the middle.

In Figs. 7 and 8, we show this construction for the present simplest case. In this case, the whole configuration is a zero-instanton-number part (surrounded by the black lines in 8), thus the possible configurations include only two types.

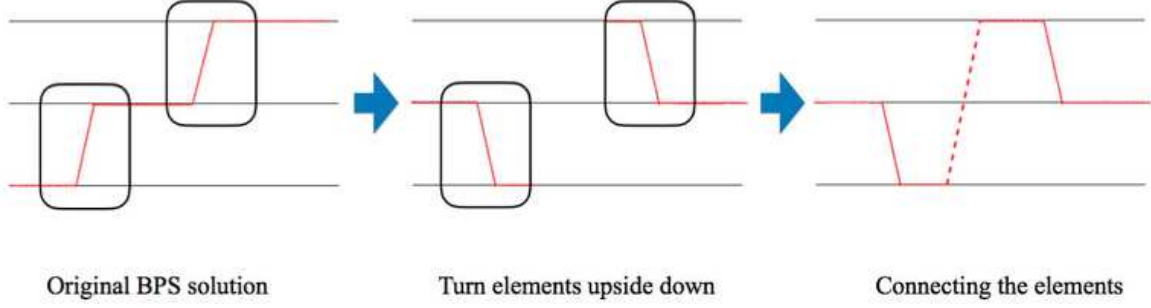


FIG. 7: Construction of the non-BPS exact solution from the BPS solution with two fractional instantons.

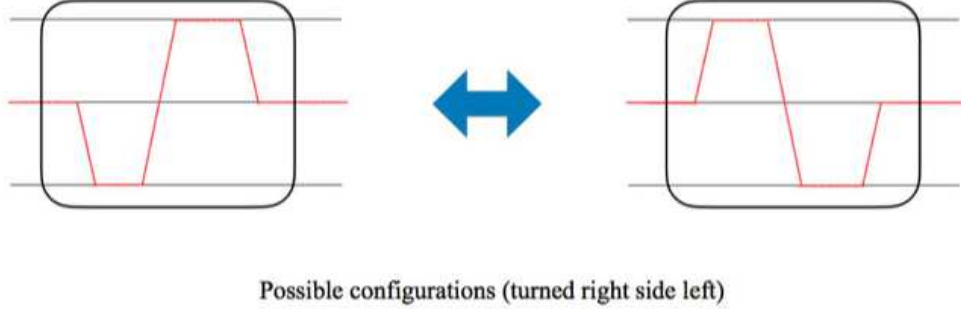


FIG. 8: Possible configurations are depicted for the non-BPS exact solution constructed from the two fractional instantons as the starting BPS solution.

We conjecture the above features are generic patterns of non-BPS exact solutions in $\mathbb{C}P^{N-1}$ model on $\mathbb{R}^1 \times S^1$ with \mathbb{Z}_N -twisted boundary condition. To check these features in other examples, we first begin with a BPS solution with three fractional instantons in the $\mathbb{C}P^3$ model.

$$\begin{aligned} \omega_{III} &= (l_1 e^{-3\beta z}, l_2 e^{-2\beta z}, l_3 e^{-\beta z}, 1) \\ &= (C(z), D(z), E(z), 1). \end{aligned} \quad (32)$$

with $\beta = 2\pi/4 = \pi/2$. The projection operation leads to the following non-BPS solution,

$$\omega_{\text{nbps}} = (C(D\bar{D} + 2E\bar{E} + 3), D(-C\bar{C} + E\bar{E} + 2), E(2C\bar{C} + D\bar{D} - 1), 3C\bar{C} + 2D\bar{D} + E\bar{E}). \quad (33)$$

In Figs. 9 and 10, we show the case for three fractional instanton constituents in the starting

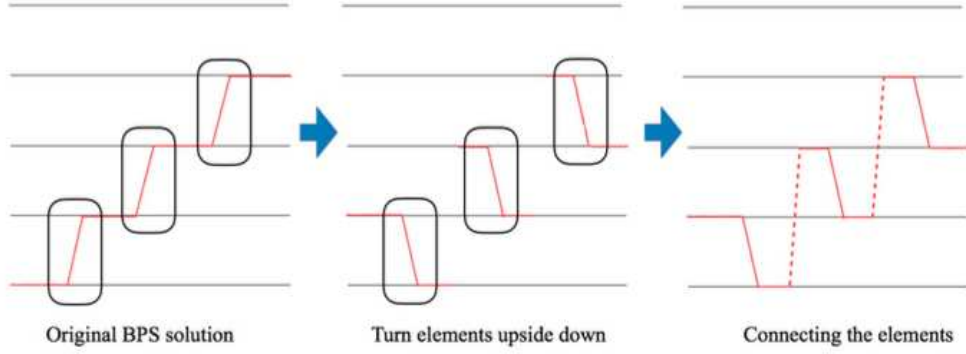


FIG. 9: Construction of the non-BPS exact solution from the BPS three fractional instanton solution \mathbb{CP}^4 model.

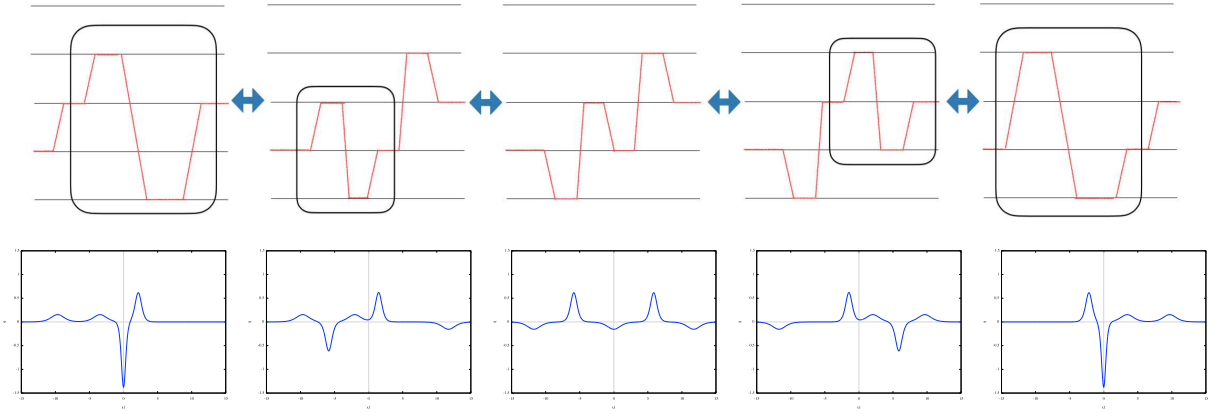


FIG. 10: Possible configurations are depicted for the non-BPS exact solution constructed from the BPS solution with three fractional instantons \mathbb{CP}^4 model.

BPS solution. (For generality, we depict the results for \mathbb{CP}^4 model with $N = 5$.) In this case, the configuration contains several zero-instanton-number parts (surrounded by the black lines in 10), thus we have five possible configurations as shown in Fig. 10. The figures in the lower row are the topological charge densities for the corresponding five parameter regions, which are calculated from (33).

Let us now temporarily think of a similar construction of the non-BPS exact solution from the BPS solution of three fractional instantons in the \mathbb{CP}^2 model ($N = 3$), instead of the $N \geq 4$ case. The BPS solution in Figs. 9 as well as non-BPS solutions in Figs. 10 now contain three fractional instantons resulting in a single instanton with $Q = 1$. Hence the action density depends on x_2 and

the instanton localizes in the two-dimensional $x_1 - x_2$ space when they get closer. Such a situation was discussed in [11].

If two fractional instantons are compressed into a single double fractional instanton in the starting BPS solution as in the left panel of Fig. 11, we find vanishing instanton charge for the non-BPS exact solution, which has only two types of configurations as in Fig. 12. It is interesting to observe that the compression of the two fractional instanton in the starting BPS solution (32) corresponds to unexpected movement of various constituents in the non-BPS solution (33) : the left-side fractional instanton moves to negative infinity. This is the reason why the topological charge in the visible (finite) region of x_1 changes from unity to zero, resulting in Fig. 12. This is a manifestation of the unusual clustering property of the non-BPS exact solutions compared to the starting BPS solutions, that was observed previously [18]. One can explain this unusual property as follows. The separation R between constituents in the starting BPS solution can be varied by varying the weight of components in the BPS solution. The separation between constituents in various configurations contained in various corners of the moduli space of the non-BPS solution are (linearly) related to the separation variables in the starting BPS solution. It is important to realize that the variable R has a simple physical meaning of separation only when it is positive. The negative values of the separation variable R between two constituents actually means the degree of compression between them, since the metric for R in such a region is cigar-like [83]. The full-compression of two constituent fractional instantons in the starting BPS solution corresponds to large negative values $R \rightarrow -\infty$. The separation variables R 's in configurations of the non-BPS solution are linearly related to R 's in the starting BPS solution. Depending on the corners of moduli spaces, they can be positive implying the corresponding constituent going to infinity. This is observed as the breakdown of clustering property. Similar phenomenon occurs between different configurations (flipping partners) contained in different corners of moduli space.

In Figs. 13 and 14, we show the construction starting from the BPS solution with one double fractional instanton and two fractional instantons. In this case, the configuration contains several zero-instanton-number parts, thus we again have five possible configurations as shown in Fig. 14.

IV. BALANCE OF FORCES IN THE NON-BPS EXACT SOLUTION

To understand the reason why no force is acting on various constituents of the non-BPS exact solution, we first analyze in terms of two-body forces between solitons in various configurations and will reveal the presence of three-body forces. We consider the $\mathbb{C}P^2$ model for simplicity.

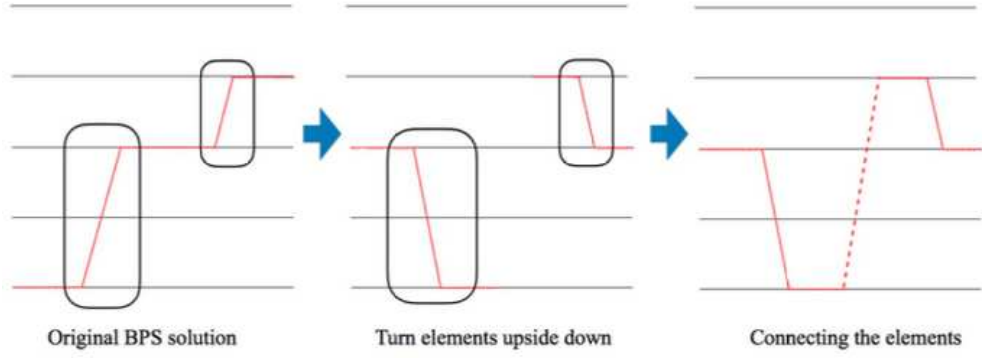


FIG. 11: Construction of the non-BPS exact solution from the BPS solution with a compressed double fractional instanton CP^4 model.

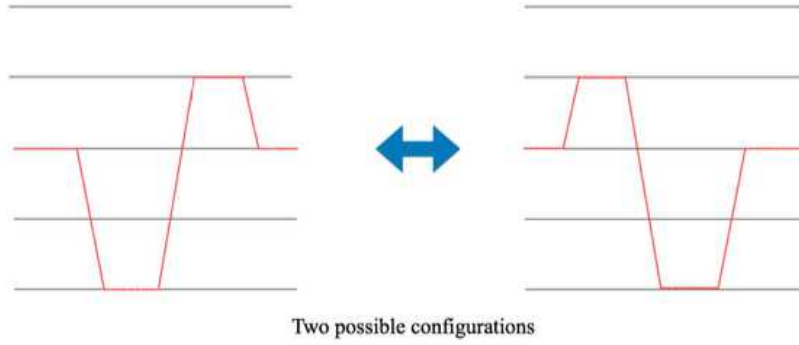


FIG. 12: Possible configurations are depicted for the non-BPS exact solution constructed from the BPS solution with one double fractional instanton and one fractional instanton for CP^4 model.

A. A bion configuration : $\bar{\mathcal{I}}\mathcal{I}$

We begin with the bion configuration in Fig. 2 as the simplest non-BPS configuration. The effective interaction potential in Eq. (12) between the two constituents for large separation R is attractive for the relative phase $|\theta_b| < \pi/2$, but is repulsive for $|\theta_b| > \pi/2$. Consequently the total action at $\theta_b = \pi/2$ is flat along the R direction for large separations, satisfying a necessary condition to be an exact solution. However, the total action has a positive θ_b derivative, and the bion cannot be a stationary point of the action. We need to remedy the strong θ_b dependence to achieve the balance of force.

These features of the two body force is clearly visible in Fig. 15, where we depict the total

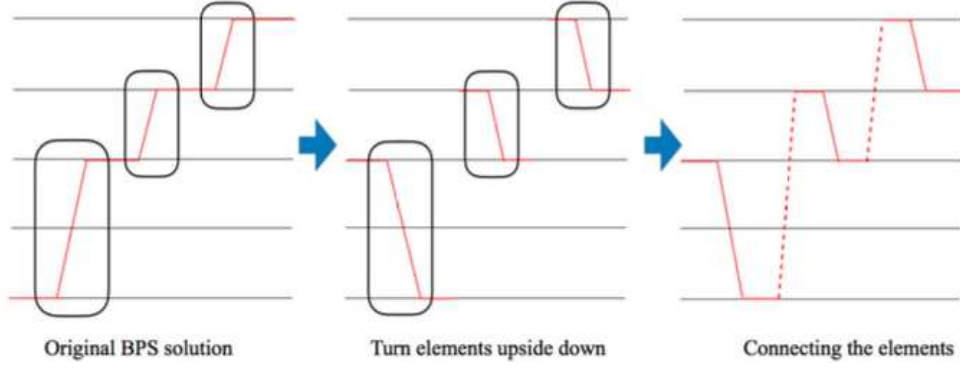


FIG. 13: Construction of the non-BPS exact solution from the BPS solution with one double fractional instanton and two fractional instantons for $\mathbb{C}P^4$ model.

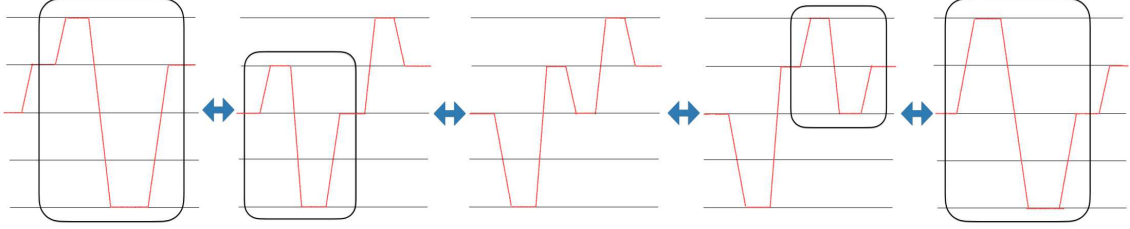


FIG. 14: Possible configurations are depicted for the non-BPS exact solution constructed from the BPS solution with one double fractional instanton and two fractional instantons for $\mathbb{C}P^4$ model.

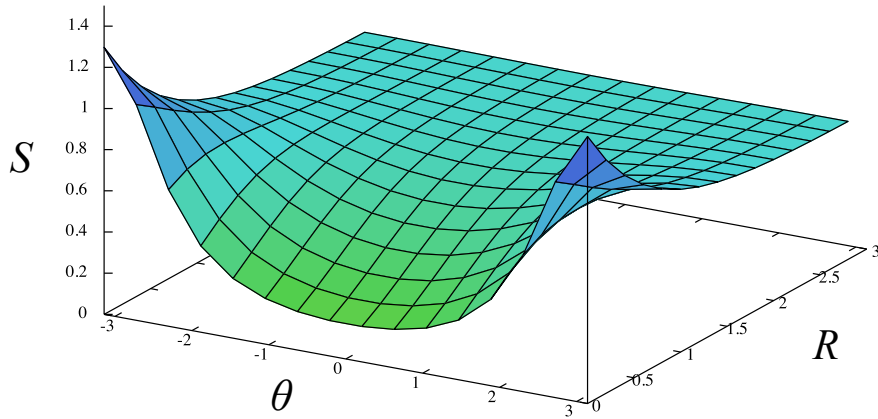


FIG. 15: The total action of bion configuration (7) as a function of the separation R and the relative phase $\theta_b \equiv \theta$ in $\mathbb{C}P^2$ model.

action of the bion in Eq. (7) as a function of the separation R and the relative phase θ_b .

B. A fractional anti-instanton and a bion : $\bar{\mathcal{I}}\bar{\mathcal{I}}\mathcal{I}$

In order to eliminate the strong dependence on the relative phase, we next consider the addition of a fractional anti-instanton to the bion configuration from the small x_1 side as shown in Fig. 16.

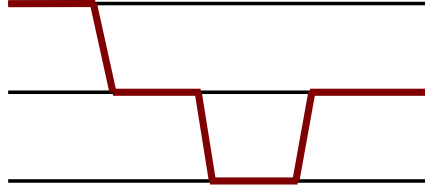


FIG. 16: The configuration of fractional anti-instanton + bion in (34) is depicted for \mathbb{CP}^2 model.

The configuration within our ansatz is given by

$$\omega_{\bar{\mathcal{I}}\bar{\mathcal{I}}\mathcal{I}} = \left(ae^{i\theta_a} e^{-\frac{2\pi}{3}z}, \quad 1 + be^{i\theta_b} e^{-\frac{2\pi}{3}(z+\bar{z})}, \quad ge^{i\theta_g} e^{-\frac{2\pi}{3}(z+2\bar{z})} \right), \quad (34)$$

with $a, b, g \in \mathbb{R}$ and $-\pi < \theta_a, \theta_b, \theta_g \leq \pi$. The action and topological charge densities are independent of θ_a and θ_g . The separation of two fractional anti-instantons in the left is $R_{\bar{\mathcal{I}}\bar{\mathcal{I}}} = \frac{3}{2\pi} \log \frac{b^2}{ag}$ and the separation between the middle fractional anti-instanton and the instanton is $R_{\text{bion}} = \frac{3}{2\pi} \log \frac{a^2}{b}$. For large separations $R_{\bar{\mathcal{I}}\bar{\mathcal{I}}}$ and R_{bion} , the total action depends only on R_{bion} and the phase θ_b , and is independent of $R_{\bar{\mathcal{I}}\bar{\mathcal{I}}}$, reflecting the absence of static forces between fractional instantons. Therefore we obtain no improvement by adding the fractional anti-instanton, as long as they are well separated.

If we let $b \rightarrow 0$ in Eq. (34), the left-most fractional instanton is compressed into the middle fractional instanton. In the completely compressed limit $b = 0$, we obtain the unnormalized vector field ω as

$$\omega_{(\bar{\mathcal{I}}\bar{\mathcal{I}})\mathcal{I}} = \left(ae^{i\theta_a} e^{-\frac{2\pi}{3}z}, \quad 1, \quad ge^{i\theta_g} e^{-\frac{2\pi}{3}(z+2\bar{z})} \right). \quad (35)$$

The configuration contains one fully-compressed double fractional anti-instanton ($\bar{\mathcal{I}}\bar{\mathcal{I}}$) and one fractional instanton \mathcal{I} as shown in Fig. 17 ($Q = 1/3$). The vacuum transitions occur $(0, 0, 1) \rightarrow$

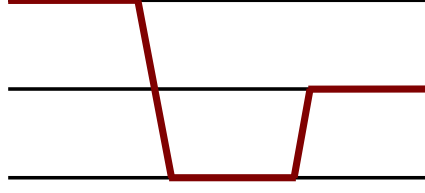


FIG. 17: The configuration (35) of a double fractional anti-instanton + a fractional instanton.

$(1,0,0) \rightarrow (0,1,0)$, as x_1 varies from $x_1 = -\infty$ to $x_1 = \infty$. The separation between the two constituents is given by $R = (3/(4\pi)) \log(a^3/g)$. We emphasize that this configuration is independent of all the phase parameters $\theta_a, \theta_b, \theta_g$, since the action density and topological charge density is independent of phases θ_a, θ_g for each component, and the phase θ_b disappears in the limit of $b \rightarrow 0$. Therefore we succeeded to eliminate the strong phase dependence of the effective interaction potential by just compressing another fractional anti-instanton with the fractional anti-instanton constituent of the bion. We can understand the disappearance of the phase dependence of the effective interaction potential when the two fractional instanton become closer (compressed), as a result of strong deformation of the internal structure of the compressed double fractional anti-instantons ($\bar{\mathcal{I}}\bar{\mathcal{I}}$) compared to two individual fractional anti-instantons. For large values of separation R , the phase dependent two-body forces like in Eq. (12) is no longer acting.

However, the approximation with two-body forces between the compressed double fractional anti-instanton and a fractional instanton is no longer valid, if we compress these two constituents further by letting a small with g (the center of mass position) fixed. In Fig. 18, we depict the action density (left) and topological charge density (right) for three values of the parameter $a = 1/100, 1/10, 100$ (from top to bottom) with $g = 1$ fixed. We can clearly see that the total action is not equal to an absolute value of the topological charge, even when the two constituents are compressed ($a = 100$).

In Fig. 19, we depict the total action as a function of the separation $R = (3/4\pi) \log(a^3/g)$. The smaller a corresponds to the smaller separation R between the constituents. The action starts from $S = 1$ and approaches a composite soliton of compressed double fractional anti-instanton and an instanton with the action $S = 5/9$ and $Q = 1/3$. Therefore the configuration experiences a (weak) attractive force at small separations R . We need more modifications of the configuration to achieve

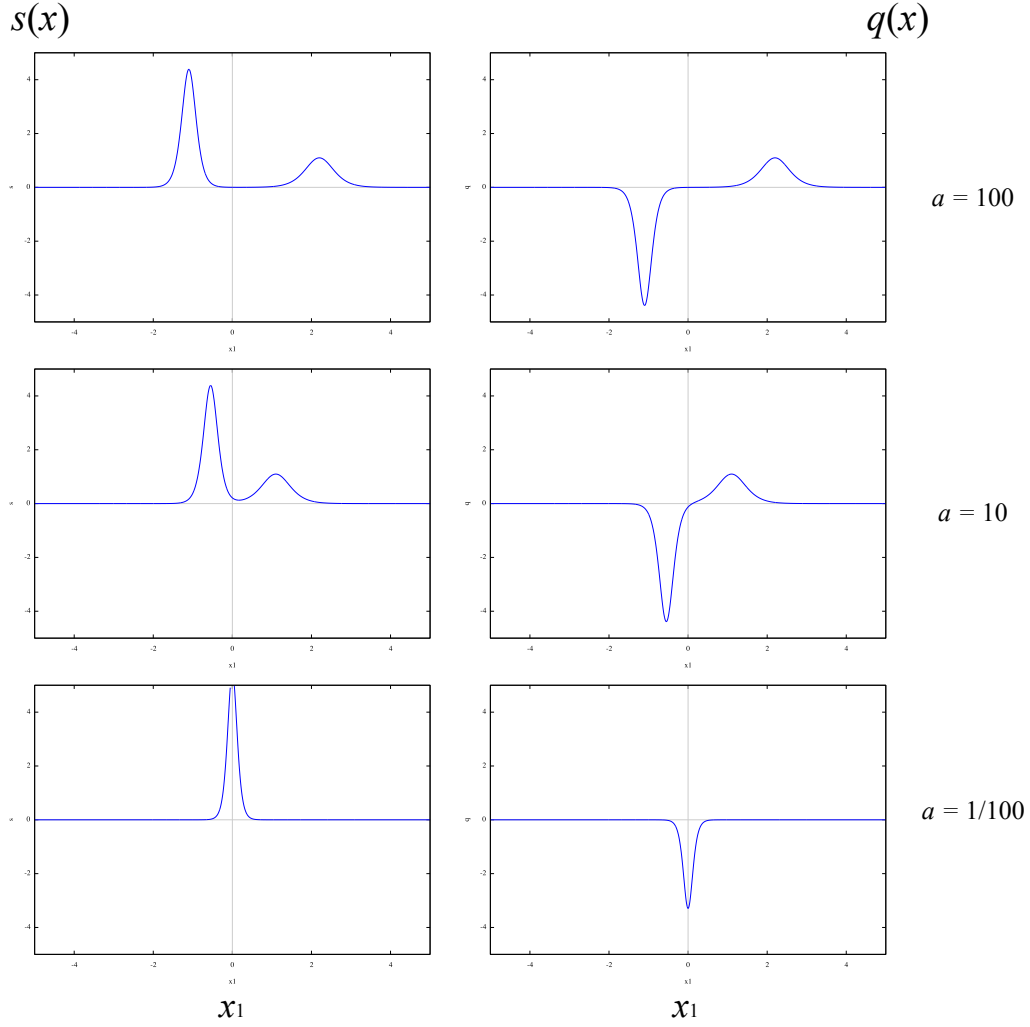


FIG. 18: The action density (left) and topological charge density (right) of the configuration $(\bar{I}\bar{I})I$ in Eq. (35) for three values of the parameter $a = 100, 10, 1/100$ (from top to bottom) with $g = 1$ fixed.

the balance of force.

C. An additional fractional instanton : $I(\bar{I}\bar{I})I$

To see the importance of considering approximation beyond the two-body forces, let us modify the configuration in Eq. (35) by adding one more fractional anti-instanton to the left of the

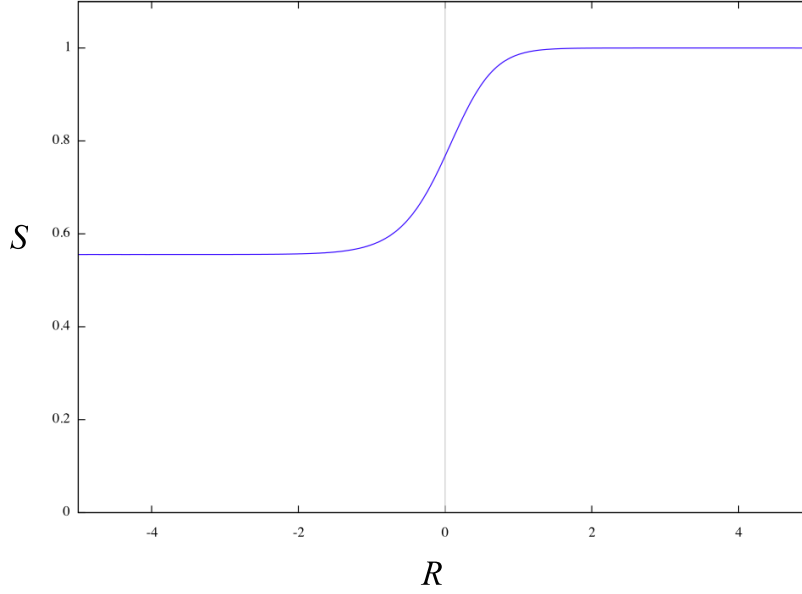


FIG. 19: The total action of the configuration $(\bar{\mathcal{I}}\bar{\mathcal{I}})\mathcal{I}$ in Eq. (35) as a function of the separation $R = (3/4\pi) \log(a^3/g)$.

compressed double fractional instanton, which can be parametrized as

$$\omega_{\mathcal{I}(\bar{\mathcal{I}}\bar{\mathcal{I}})\mathcal{I}} = \left(ae^{-\frac{2\pi}{3}z}, \quad 1 + de^{i(\theta+\pi)}e^{-\frac{4\pi}{3}(z+\bar{z})}, \quad ge^{-\frac{2\pi}{3}(z+2\bar{z})} \right). \quad (36)$$

We omit the irrelevant phase factor in the first component, and redefine the relative phase in the second component as $\theta \rightarrow \theta + \pi$, for later convenience. The configuration $\mathcal{I}(\bar{\mathcal{I}}\bar{\mathcal{I}})\mathcal{I}$ consists of a compressed double fractional anti-instanton $(\bar{\mathcal{I}}\bar{\mathcal{I}})$ sandwiched between fractional instantons and looks very similar to Fig. 5(a), one of configurations contained in the simplest non-BPS exact solution (20) with $S = 4/3, Q = 0$. The action density depends on the relative phase θ in the second component, the separation $R_1 = (3/4\pi) \log(g^3/(ad^2))$ between $(\bar{\mathcal{I}}\bar{\mathcal{I}})$ and the left fractional instanton and the separation $R_2 = (3/4\pi) \log(a^3/g)$ between $(\bar{\mathcal{I}}\bar{\mathcal{I}})$ and the right fractional instanton.

If we restrict the three parameters a, d, g in terms of two parameters l_1, l_2 as $a = 2l_1/l_2$, $d = l_1^2$, $g = -2l_1^2/l_2$, we obtain

$$\omega_{\mathcal{I}(\bar{\mathcal{I}}\bar{\mathcal{I}})\mathcal{I}} = \left(\frac{2l_1}{l_2}e^{-\frac{2\pi}{3}z}, \quad 1 - l_1^2e^{i\theta}e^{-\frac{4\pi}{3}(z+\bar{z})}, \quad -\frac{2l_1^2}{l_2}e^{-\frac{2\pi}{3}(z+2\bar{z})} \right). \quad (37)$$

If the phase θ vanishes, the configuration becomes equivalent to dominant terms of the non-BPS exact solution (20) in a parameter region $2l_1 \gg l_2^2$, representing one of the configurations in Fig. 5(a). We see that two separations are equal : $R = R_1 = R_2 = (3/4\pi) \log(4l_1/l_2^2)$. Thus, the

energy density is symmetric under the reflection around the middle compressed double fractional instanton. We call this symmetry as *reflection symmetry*. If the reflection symmetry is broken, the balance of force fails, as we will see later. Thus, the reflection symmetry is one of the essential properties of the non-BPS exact solutions.

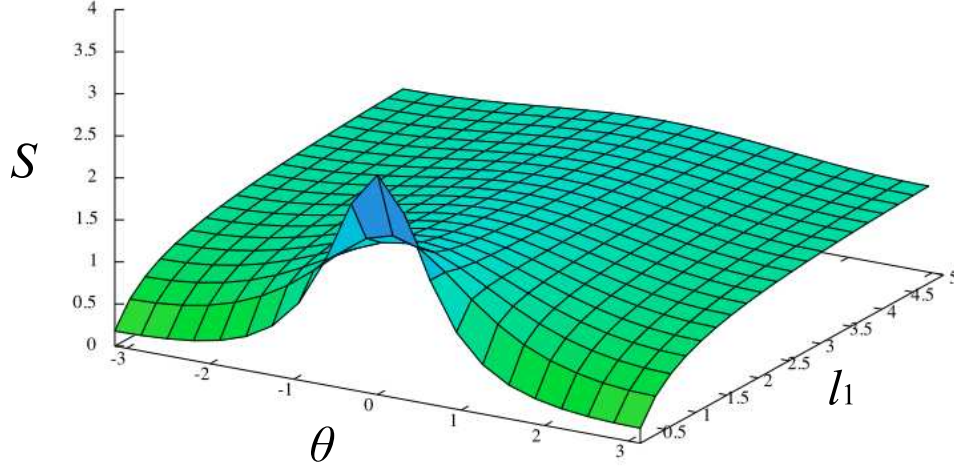


FIG. 20: The total action of the configuration $\mathcal{I}(\bar{\mathcal{I}}\bar{\mathcal{I}})\mathcal{I}$ in Eq. (37) as a function of the phase parameter θ and the separation parameter l_1 with $l_2 = 1$ fixed: $R = (3/4\pi) \log(4l_1/l_2^2)$.

Fig. 20 shows the total action of (37) as a function of the phase parameter θ and the parameter l_1 with $l_2 = 1$ fixed, which gives the separation $R = (3/4\pi) \log(4l_1/l_2^2)$. For $\theta = \pi$, in which the two terms in the second component in (37) have the same sign, the action decreases most rapidly as l_1 gets smaller (R gets smaller), thus the effective force is attractive. For $\theta = 0$, in which the two terms in the second component have the opposite sign, the action increases as l_1 gets smaller (R gets smaller), thus the effective force is repulsive. If one wants to achieve the balance of force to obtain a solution of field equations, it is a fatal flaw to have an attractive interaction, since the configuration tends to decay into vacuum in our case of topologically trivial sector. This is in accordance with the sign of the two terms of the second component in the non-BPS exact solution (20).

It is important to realize that the force we have discussed here is a three-body force involving three constituent solitons : θ is the relative phase between the two terms corresponding to the left-most and right-most vacua. If one focuses on the two constituents, for example, the left anti-instanton and central double instanton, they have attractive force for any θ (only at small separations), as we have seen. Moreover, the reflection symmetry is also important, since the

two-body force between constituents with shorter separation dominates to give the attractive force whenever the reflection symmetry is broken. This is why the reflection symmetry is also essential in the non-BPS exact solution.

Now, the only question is how the non-BPS exact solution suppresses the repulsive force resulting in the total action $S = 4/3$ for any values of R at $\theta = 0$ and the vanishing derivative with respect to θ . Compared to the present case, the non-BPS exact solution (20) has the other terms, which produce the flipping-partner configuration for $l_2^2 > 2l_1$ as shown in Fig. 5. We have to conclude that these terms for the flipping partner also work to avoid the increase of the total action for the parameter range $2l_1 > l_2^2$, even though these terms appear to be irrelevant at a glance. Thus, the existence of flipping partners is also essential in the non-BPS exact solution.

D. Essential properties of non-BPS exact solutions

To sum up, we list essential properties of the non-BPS exact solution (20), which give the constant total action without annihilation into vacuum in the entire moduli space.

1. Relative sign

The terms in the solution have the appropriate relative signs : these signs serve to suppress the dominant two-body attractive forces, and to provide many-body repulsive forces suppressing a decay into vacuum.

2. Reflection symmetry

The reflection symmetry around the middle compressed double fractional instanton prevents the dominance of attractive two-body forces.

3. Flipping partner

The non-BPS exact solution makes a transition between two seemingly different configurations (flipping partners), as moduli parameters are varied across the point where all the constituents get closer. They never annihilate each other even though no topological quantum number guarantees the flatness of the total action. This transition is essential to provide the many-body forces to cancel the two-body and three-body forces in configurations without the flipping partners.

All the configurations we have discussed including the non-BPS exact solutions correspond to some special cases of the generic two-bion ansatz in (13). We emphasize that this ansatz provides

the multi-instanton computation needed to achieve the resurgence. Therefore, the non-BPS exact solutions contribute to a part of the multi-instanton moduli integral relevant to the resurgence theory.

V. LOCAL AND GLOBAL STABILITY

It has been pointed out that the non-BPS exact solutions have unstable modes [76]. In this section, we analyze the local stability of the non-BPS exact solution in Eq. (20) to understand the physical meaning of unstable negative modes within the parametrization of our general ansatz in Eq. (13). We focus only on the simplest non-BPS solution in the \mathbb{CP}^2 model. As we see in Sec. II A, this ansatz has nine dimensional space of relevant parameters : four relative phases and five separations. However, different sets of parameters are relevant to analyze the stability of four different configurations in Fig. 3(a), (b), (c), and (d). We need to concentrate on two types of configurations (b) and (c), since only these two (flipping partners) arise in the vicinity of the non-BPS exact solution. The configuration in Fig. 3(b) depends on only two phases b and d , and three separations $R'_{21}, R'_{32}, R'_{43}$. Another configuration in Fig. 3(c) can be obtained by the reflection symmetry. Therefore we need to consider only the five dimensional parameter space. The other two relative phases (a, c) and (f, g) are only relevant to examine the two (anti-)bion configurations in Fig. 3(a) and (d), which requires large deformations from the non-BPS exact solution. We also examine globally other possible saddle points within our ansatz, to which the exact solution can reach along these negative modes.

A. Phase negative modes I

In this subsection we violate the first of the essential properties (*relative sign*) of non-BPS solutions by introducing a phase θ to a term in the second component of the exact solution in Eq. (21), keeping the common separation R for left and right separations (reflection-symmetry)

$$\omega = \left(\frac{2l_1}{l_2} e^{-\frac{2\pi}{3}z} + l_1 l_2 e^{-\frac{2\pi}{3}(2z+\bar{z})}, \quad 1 - e^{i\theta} l_1^2 e^{-\frac{4\pi}{3}(z+\bar{z})}, \quad -l_2 e^{-\frac{2\pi}{3}\bar{z}} - \frac{2l_1^2}{l_2} e^{-\frac{2\pi}{3}(z+2\bar{z})} \right). \quad (38)$$

We here omit the common phases θ_1, θ_2 of the two terms in the first and second components which are included in (20), since the above configurations are independent of them. The argument in Sec. IV C suggests that the total action decreases due to the attractive force between the constituents if we flip the relative sign ($\theta = 0 \rightarrow \pi$) between the second component in (20). In Fig. 21, we show the total action as a function of the phase θ and l_2 with $l_1 = 1$ fixed (we note $R = (3/4\pi) \log(l_2^2/l_1)$)

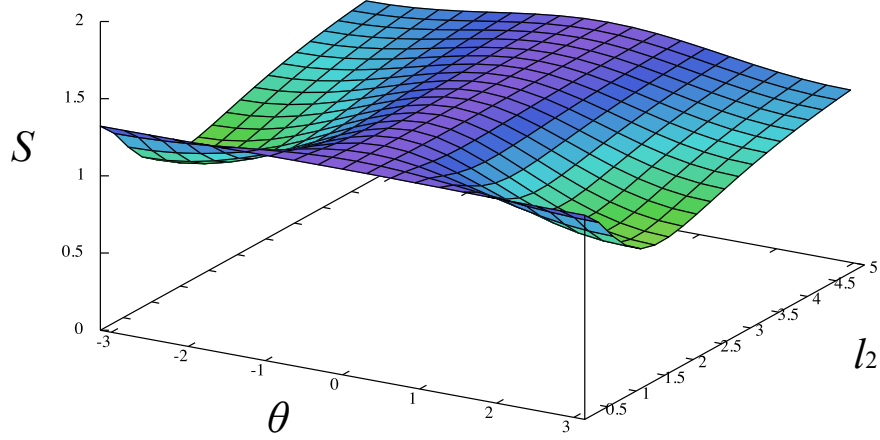


FIG. 21: The total action for the configuration in Eq. (38) as a function of θ and l_2 with $l_1 = 1$ fixed (we note $R = (3/4\pi) \log(l_2^2/l_1)$ for $l_2^2 > 2l_1$).

for $l_2^2 > 2l_1$). We also display the total action as a function of θ with the fixed separation $l_1 = 1, l_2 = 1$ in Fig. 22. We find that the total action decreases when we change θ from 0 to π , indicating a negative mode along θ direction. For the large separation $2l_1 \gg l_2^2$ or $2l_1 \ll l_2^2$, the total action dependence on θ becomes small (but exists), since the magnitude of the two-body force decreases for small separations.

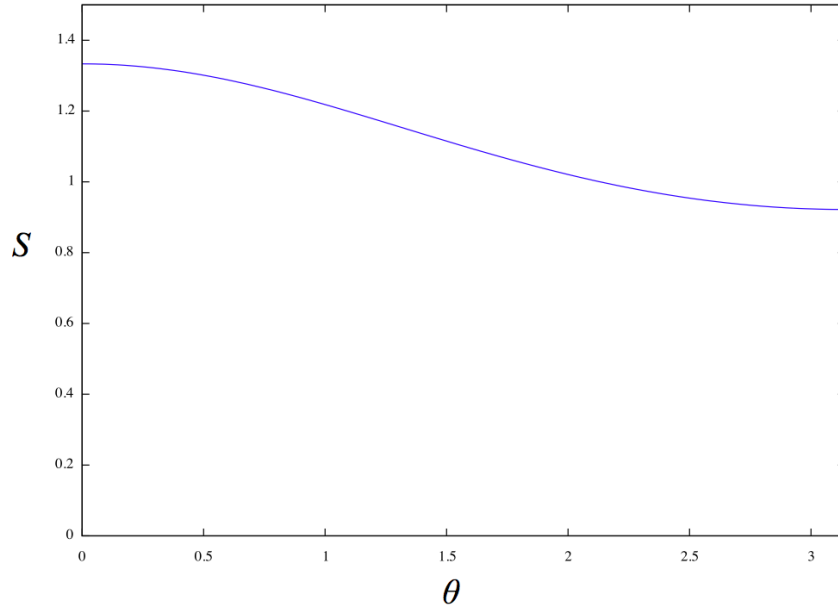


FIG. 22: The total action of the configuration in Eq. (38) as a function of θ with $l_1 = l_2 = 1$ fixed.

B. Negative modes for asymmetric separation

In this subsection we violate the second of the essential properties (*reflection symmetry*) of the non-BPS exact solution by introducing two multiplicative factors $\gamma, \gamma' \in \mathbb{R}$ in order to change the left and right separations

$$\omega = \left(\frac{2l_1}{l_2} e^{-\frac{2\pi}{3}z} + l_1 l_2 e^{-\frac{2\pi}{3}(2z+\bar{z})}, \quad \gamma' - \gamma l_1^2 e^{-\frac{4\pi}{3}(z+\bar{z})}, \quad -l_2 e^{-\frac{2\pi}{3}\bar{z}} - \frac{2l_1^2}{l_2} e^{-\frac{2\pi}{3}(z+2\bar{z})} \right). \quad (39)$$

For $\gamma, \gamma' \neq 1$, the configurations are no longer solutions.

In the parameter region $2l_1 > l_2^2$, we have a configuration similar to that in Fig. 5(a). However, the separation

$$R_L = \frac{3}{4\pi} \log\left(\frac{4l_1}{\gamma^2 l_2^2}\right), \quad (40)$$

between the left instanton and the middle compressed double anti-instanton is decreased by $\gamma > 1$. Similarly, the separation

$$R_R = \frac{3}{4\pi} \log\left(\frac{4l_1}{\gamma'^2 l_2^2}\right), \quad (41)$$

between the middle compressed double anti-instanton and the right instanton is decreased by $\gamma' > 1$.

In the parameter region $2l_1 < l_2^2$, we have another configuration similar to that in Fig. 5(b). The separation

$$R'_L = \frac{3}{4\pi} \log\left(\frac{l_2^2}{\gamma^2 l_1}\right), \quad (42)$$

between the left anti-instanton and the middle compressed double instanton is decreased by $\gamma > 1$, and the separation

$$R'_R = \frac{3}{4\pi} \log\left(\frac{l_2^2}{\gamma'^2 l_1}\right), \quad (43)$$

between the middle compressed double instanton and the right anti-instanton is decreased by $\gamma' > 1$.

Fig. 23 shows the action and topological charge densities of the configuration in Eq. (39) with $\gamma > 1, \gamma' = 1$ and $2l_1 < l_2^2$. When the right separation R'_R is large and fixed, we can regard the configuration as the addition of noninteracting fractional anti-instanton to the configuration of compressed double fractional instanton and an anti-instanton similar to that in Eq. (35). Therefore,

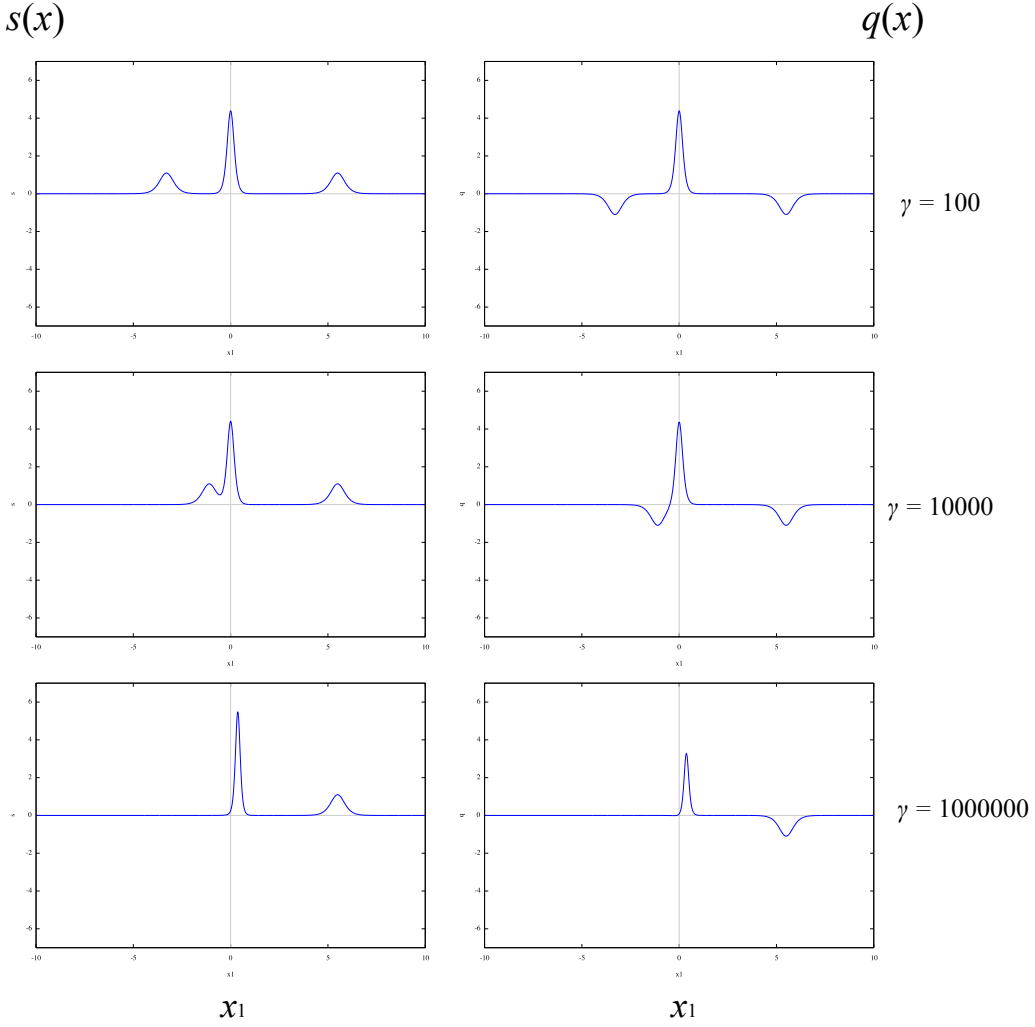


FIG. 23: The action density and topological charge density of the configuration in Eq. (39) are shown in left and right columns, respectively. From top to bottom, densities are shown for three values of the parameter $\gamma = 100, 10000, 1000000$, with $\gamma' = 1$ and $l_1 = 1$ $l_2 = 100000$ fixed.

the total action, which is originally $S = 4/3$ for the non-BPS exact solution (20), decreases and ends up with

$$S = 5/9 + 1/3 = 8/9, \quad (44)$$

for the $\gamma \rightarrow \infty$ limit, where the left fractional anti-instanton is fully compressed with the double fractional instanton. The value $5/9$ of the action comes from the compressed part of fractional anti-instanton + double fractional instanton as found in Fig. 19.

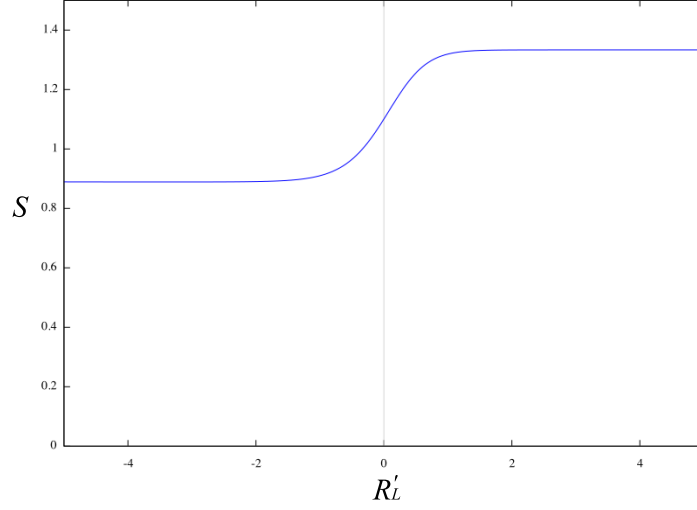


FIG. 24: Total action of configuration in Eq. (39) as a function of $R'_L = \frac{3}{4\pi} \log \frac{l_2^2}{\gamma'^2 l_1}$ with $\gamma' = 1$, $l_1 = 1$, $l_2 = 10000$ fixed. The non-BPS solution with $\gamma = 1$ correspond to $R'_L \sim 4.4$

Figure 24 shows the total action as a function of separation R_L in Eq. (40) between the left anti-instanton and the middle double fractional instanton. Thus we find that increasing γ with $\gamma' = 1$ fixed is a negative mode. Moreover, the increase of γ leads to a configuration of fully compressed fractional instanton + double fractional anti-instanton together with a (almost) noninteracting fractional instanton to their right.

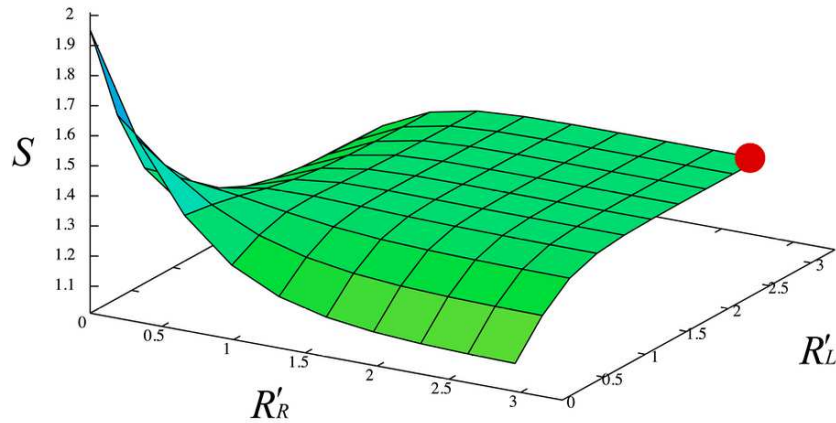


FIG. 25: The total action as a function of $R'_R = \frac{3}{4\pi} \log \frac{l_2^2}{\gamma'^2 l_1}$ and $R'_L = \frac{3}{4\pi} \log \frac{l_2^2}{\gamma^2 l_1}$ for (45) with $\theta = 0$. In the calculation, we fix $l_1 = 1$ and $l_2 = 1000$, and vary γ, γ' . The non-BPS solution (which means $\gamma = \gamma' = 1$) corresponds to $R'_R = R'_L \sim 3.3$, the red point at the corner.

Similarly, increasing γ' with γ fixed is found to be a negative mode, leading to a configuration of fully compressed fractional double fractional anti-instanton + instanton together with a (almost) noninteracting fractional instanton to their left.

We next consider the deformation combining (38) and (39),

$$\omega = \left(\frac{2l_1}{l_2} e^{-\frac{2\pi}{3}z} + l_1 l_2 e^{-\frac{2\pi}{3}(2z+\bar{z})}, \quad \gamma' - \gamma e^{i\theta} l_1^2 e^{-\frac{4\pi}{3}(z+\bar{z})}, \quad -l_2 e^{-\frac{2\pi}{3}\bar{z}} - \frac{2l_1^2}{l_2} e^{-\frac{2\pi}{3}(z+2\bar{z})} \right). \quad (45)$$

As we have discussed in the previous section, this configuration behaves differently with $\theta = 0$ and $\theta = \pi$. In both cases, the increase of $\gamma > 1$ with $\gamma' = 1$ or the increase of $\gamma' > 1$ with $\gamma = 1$ decreases the total action from $S = 4/3$ to $S = 8/9$ since the double fractional instanton and the fractional anti-instanton at each side have attractive interaction. However, things change if one increases both γ and γ' with $\gamma = \gamma'$.

For $\theta = 0$, the three instanton constituents have effectively repulsive interaction as we have seen in Fig. 20. Thus the total action increases as one increases $\gamma = \gamma' > 1$. In Fig. 25, we depict the total action as a function of $R'_R = \frac{3}{4\pi} \log \frac{l_2^2}{\gamma'^2 l_1}$ and $R'_L = \frac{3}{4\pi} \log \frac{l_2^2}{\gamma^2 l_1}$. In the calculation, we fix $l_1 = 1$ and $l_2 = 1000$, and vary γ, γ' . Along $R'_R = R'_L \rightarrow 0$, the action increases.

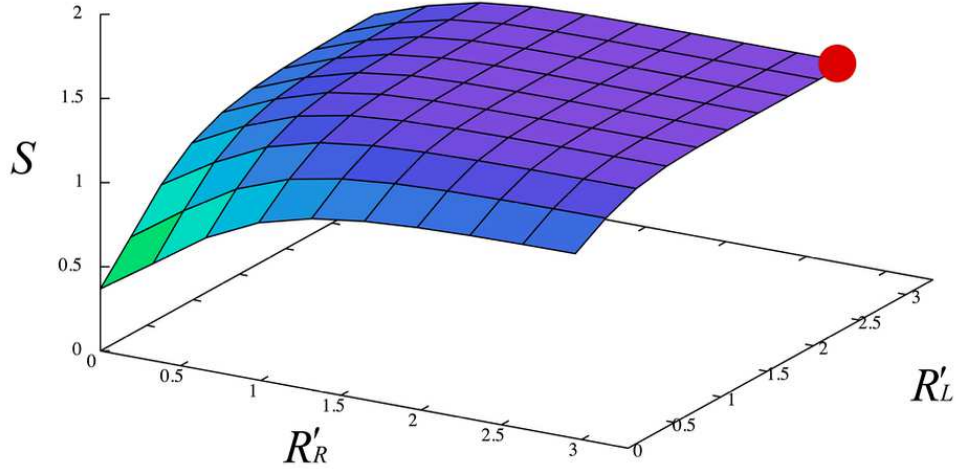


FIG. 26: The total action of Eq. (45) as a function of $R'_R = \frac{3}{4\pi} \log \frac{l_2^2}{\gamma'^2 l_1}$ and $R'_L = \frac{3}{4\pi} \log \frac{l_2^2}{\gamma^2 l_1}$ for (45) with $\theta = \pi$. In the calculation, we fix $l_1 = 1$ and $l_2 = 1000$, and vary γ, γ' . The red point corresponds to $\gamma = \gamma' = 1$.

For $\theta = \pi$, the three instanton constituents have effectively attractive interaction. Thus the total action decreases as one increases $\gamma = \gamma' > 1$. In Fig. 26, we depict the total action as a function of R'_R and R'_L , where we fix $l_1 = 1$ and $l_2 = 1000$, and vary γ, γ' . In any direction of

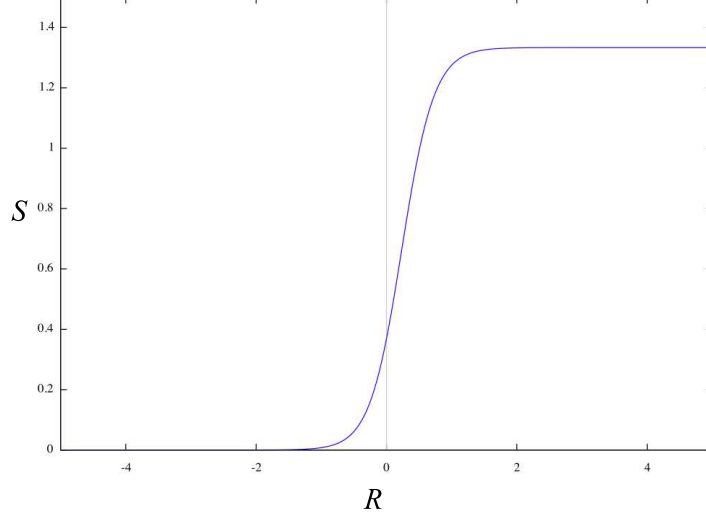


FIG. 27: The total action of Eq. (45) as a function of $R = R'_R = R'_L$ keeping $\theta = \pi$ with $l_1 = 1$, $l_2 = 100000$ fixed.

decreasing R'_R, R'_L (increasing γ, γ') from the original configuration, the action decreases. Figure 27 shows the total action as a function of $R = R'_R = R'_L$, showing clearly that the total action decreases to $S = 0$ towards $R = R'_R = R'_L \rightarrow -\infty$. (This corresponds to the curve obtained as a section along $R'_R = R'_L$ in Fig. 26 although we change the parameter value in the two figures.) In Fig. 28, corresponding to (45) with $2l_1 < l_2^2$, we depict how the instanton constituents meet and are compressed when $\gamma = \gamma'$ increases.

C. Number and directions of negative modes

Before discussing the directions associated to the remaining parameters, we quantify the mass squared matrix of fluctuations around the non-BPS exact solution to find the number and directions of negative modes described by γ, γ', θ in Eq. (45). As a natural coordinates of the parameter space, we take R'_R, R'_L, θ , since they are associated to the flat metric for kinetic terms at least for large separations. For small separations, their physical meaning are admittedly less clear. The mass squared matrix is given by the 3×3 matrix of second-derivatives. Diagonalization of the matrix gives the number of mass squared eigenvalues and the direction of eigenmodes.

We consider the three sets of the parameters in the non-BPS solution $l_2 = 100, 10, 1$ with $l_1 = 1$ fixed, which correspond to the cases that the separation between the double fractional instanton and the fractional anti-instantons at the both side are $R \sim 2.20, 1.10, 0$.

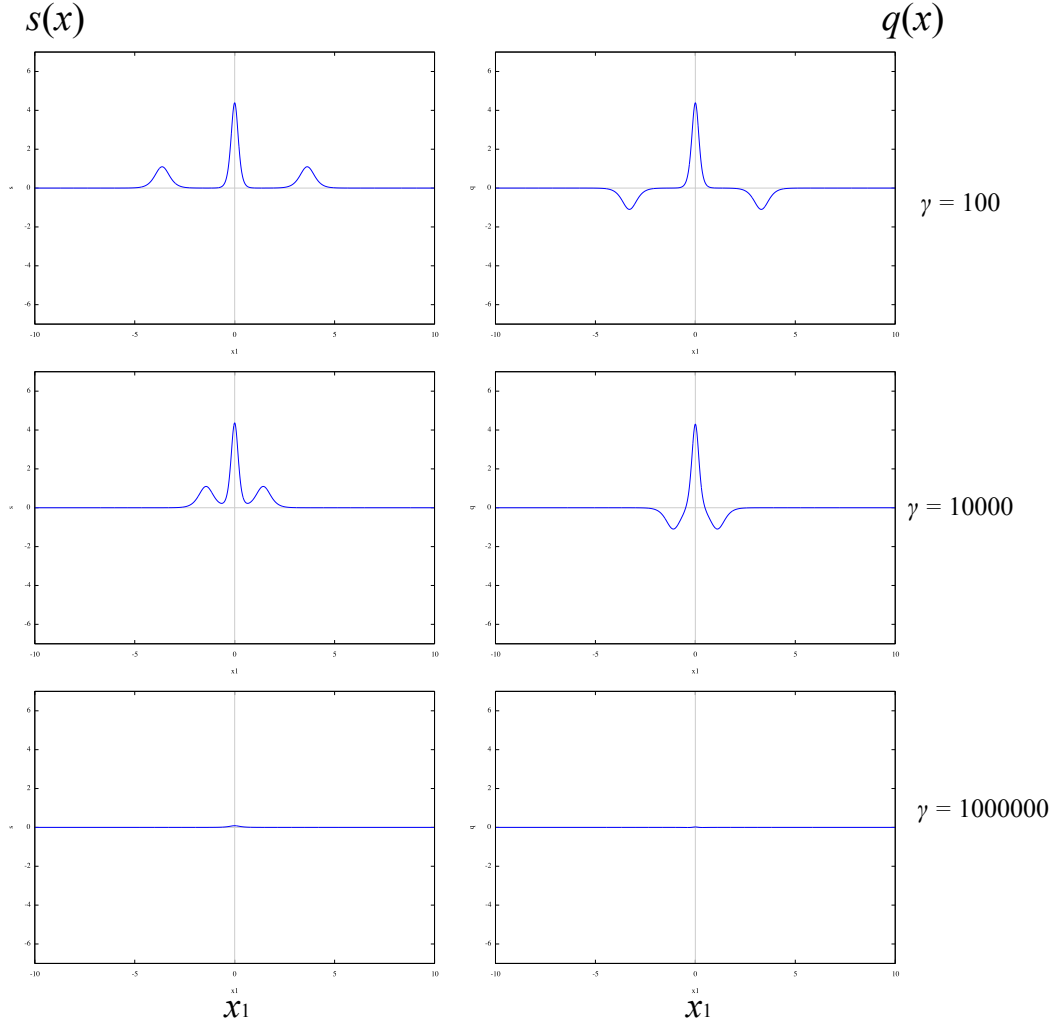


FIG. 28: Action density (left) and topological charge density (right) of Eq. (45) for three values of parameter $\gamma = \gamma' = 100, 10000, 1000000$ (from top to bottom) with $l_1 = 1, l_2 = 100000, \theta = \pi$ fixed.

For $R = 2.20$ ($l_2 = 100, l_1 = 1$), the separation is relatively large. The second-derivative matrix at $\gamma = 1, \gamma' = 1, \theta = 0$ is numerically calculated as

$$\frac{\partial^2 S}{\partial(R'_R, R'_L, \theta)^2} \approx \begin{pmatrix} -9.11 & 9.17 & O(10^{-3}) \\ 9.17 & -9.11 & O(10^{-3}) \\ O(10^{-3}) & O(10^{-3}) & -2.11 \end{pmatrix} \times 10^{-4}, \quad (46)$$

where the label R'_R, R'_L, θ stands for the ordering of rows and columns. By denoting the unit

vectors as $\mathbf{e}_R, \mathbf{e}_L, \mathbf{e}_\theta$ respectively, we approximately obtain the eigenvalues and the eigenvectors as

$$\sim 6.00 \times 10^{-6} : \mathbf{e}_R + \mathbf{e}_L \quad (47)$$

$$\sim -1.83 \times 10^{-3} : \mathbf{e}_R - \mathbf{e}_L \quad (48)$$

$$\sim -2.11 \times 10^{-4} : \mathbf{e}_\theta. \quad (49)$$

We find that there are two negative modes in $\mathbf{e}_R - \mathbf{e}_L$ and \mathbf{e}_θ directions in this case.

For $R = 1.10$ ($l_2 = 10, l_1 = 1$), the separation is relatively small and the constituents are about to crash. The second-derivative matrix at $\gamma = 1, \gamma' = 1, \theta = 0$ is numerically calculated as

$$\frac{\partial^2 S}{\partial(R'_R, R'_L, \theta)^2} \approx \begin{pmatrix} -0.0606 & 0.0852 & O(10^{-6}) \\ 0.0852 & -0.0606 & O(10^{-6}) \\ O(10^{-6}) & O(10^{-6}) & -0.0204 \end{pmatrix}. \quad (50)$$

Then the eigenvalues and the eigenvectors are approximately given by

$$\sim 0.0246 : \mathbf{e}_R + \mathbf{e}_L \quad (51)$$

$$\sim -0.1458 : \mathbf{e}_R - \mathbf{e}_L \quad (52)$$

$$\sim -0.0204 : \mathbf{e}_\theta. \quad (53)$$

In this case too, we find that there are two negative modes in $\mathbf{e}_R - \mathbf{e}_L$ and \mathbf{e}_θ directions.

For $R = 0$ ($l_2 = 1, l_1 = 1$), the separation is zero and the constituents crash. The second-derivative matrix at $\gamma = 1, \gamma' = 1, \theta = 0$ is numerically calculated as

$$\frac{\partial^2 S}{\partial(R'_R, R'_L, \theta)^2} \approx \begin{pmatrix} 0.664 & 0.639 & O(10^{-5}) \\ 0.639 & 0.664 & O(10^{-5}) \\ O(10^{-5}) & O(10^{-5}) & -0.267 \end{pmatrix}. \quad (54)$$

Then the eigenvalues and the eigenvectors are approximately given by

$$\sim 1.303 : \mathbf{e}_R + \mathbf{e}_L \quad (55)$$

$$\sim 0.025 : \mathbf{e}_R - \mathbf{e}_L \quad (56)$$

$$\sim -0.267 : \mathbf{e}_\theta. \quad (57)$$

In this case, there is one negative mode in \mathbf{e}_θ directions. We should mention that coordinates R'_R and R'_L do not have a simple physical meaning as separations at small R region such as $R = 0$.

These results show that the number of negative modes depends on the parameter region. However, the relative phase fluctuation always gives a negative mode.

D. Splitting of two bions

To analyze the stability of the non-BPS exact solution, we still need to consider two more parameters : a separation parameter corresponding to the splitting of the middle compressed double fractional (anti-)instanton, and its associated phase. The splitting can be described by the following ansatz containing a new term with the parameter $\delta e^{i\theta'}$ in the second component

$$\omega = \left(\frac{2l_1}{l_2} e^{-\frac{2\pi}{3}z} + l_1 l_2 e^{-\frac{2\pi}{3}(2z+\bar{z})}, \quad 1 + \delta e^{i\theta'} e^{-\frac{2\pi}{3}(z+\bar{z})} - l_1^2 e^{-\frac{4\pi}{3}(z+\bar{z})}, \quad -l_2 e^{-\frac{2\pi}{3}\bar{z}} - \frac{2l_1^2}{l_2} e^{-\frac{2\pi}{3}(z+2\bar{z})} \right). \quad (58)$$

with $\delta \geq 0$, $0 \leq \theta' < 2\pi$. For $\delta \neq 0$, the configuration is no longer a solution. In the limit of the exact solution ($\delta = 0$), the phase θ' obviously is ill-defined and loses a physical meaning. Therefore we consider here only deformations due to these new parameters δ, θ' and postpone the analysis combined with other parameters to the next subsection.

A nonzero δ splits the double fractional (anti-)instanton in the middle of Fig. 5 into two fractional (anti-)instantons, and leads to the two bion configurations as shown in Fig. 3(b) and (c).

We first study the case of large separations between all constituents, where the two-body forces [19] in Eq. (12) between fractional instanton and anti-instanton is applicable. Since two-body forces are attractive (repulsive) for the relative phase smaller (larger) than $\pi/2$, we find that the effective forces between the fractional constituents in both two bions in Fig. 3(b) and (c) become attractive for any values of δ , only at $\theta' = \pi/2$. This is because some of the terms in (58) have relative signs, in such a way that one of the constituent pairs has an attractive interaction while the other has a repulsive interaction for $\theta' \neq \pi/2$. One should note that two fractional (anti-)instantons experience no static force because they are mutually BPS.

For example, let us consider the parameter region $2l_1 < l_2^2$, corresponding to Fig. 3(b). The fractional anti-instanton in the left end is located at $\frac{3}{2\pi} \log \frac{l_1}{l_2}$, whereas the left fractional instanton emerging from the middle double instanton is located at $\frac{3}{2\pi} \log \frac{l_1 l_2}{\delta}$. They have a relative phase $e^{i\pi}/e^{i\theta'} = e^{i(\pi-\theta')}$, and compose a left bion. Thus the constituents have an attractive force for $|\theta'| > \pi/2$, and repulsive for $|\theta'| < \pi/2$. Similarly, the fractional instanton and anti-instanton in the right bion have a relative phase $e^{i\theta'}$, and exhibit an attractive force for $|\theta'| < \pi/2$, and repulsive for $|\theta'| > \pi/2$. If $|\theta'| = \pi/2$ and the separation is small, which is beyond the scope of the two-body force approximation, the strong attractive force between the constituents of bions emerges as shown in Fig. 15. Therefore attractive forces are the strongest around $\theta' = \pm\pi/2$ since constituents of both bions are attractive for small separation only at these parameters.

We note that, for $2l_1 > l_2^2$, the situation is similar.

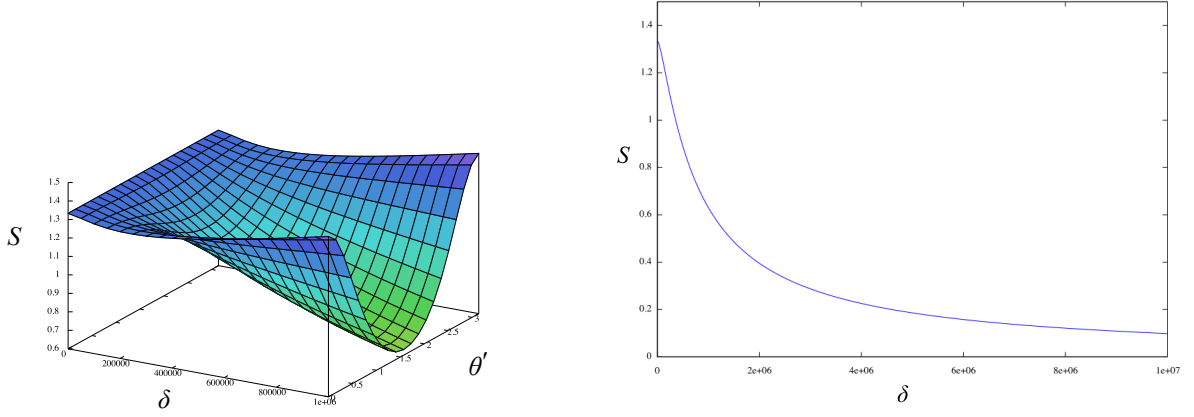


FIG. 29: The total action as a function of δ and θ' in the modified configuration (58) for $l_1 = 1, l_2 = 100$ (left). The total action as a function of δ with $\theta' = \pi/2$ fixed is also depicted (right).

In Fig 29 and Fig. 30, the total action is depicted as a function of δ and θ' for fixed l_1 and l_2 . One can see that, for $\theta' = 0, \pi$, the total action decreases at first as δ gets nonzero, then at some point it takes a turn and increases. It means that, for these values of θ' , the effective force between the fractional instanton and anti-instanton is changed from attractive to repulsive ones at some value of δ . Here we used the parameter δ instead of R to describe the length of the middle vacuum region between the two fractional instantons, since the metric for the two BPS solitons is typically cigar-like and δ is more appropriate at small separations [83].

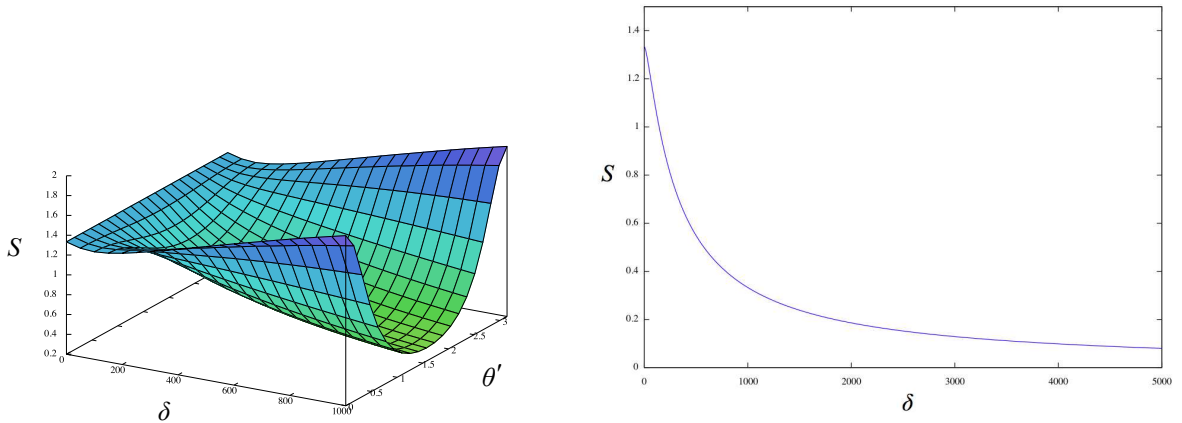


FIG. 30: The total action as a function of δ and θ' in the modified configuration (58) for $l_1 = 1, l_2 = 1/100$ (left). The total action as a function of δ with $\theta' = \pi/2$ fixed is also depicted (right).

Our observation shows that, for example, if we fix $\theta' = \pi/2$, the parameter δ is identified as one

of the unstable modes, which connects the non-BPS solution and the two bion configuration. We show how the action density changes with δ for $\theta = \pi/2$ in Fig. 31. In both left and right bions, the fractional constituents gradually annihilate into vacuum as they approach each other.

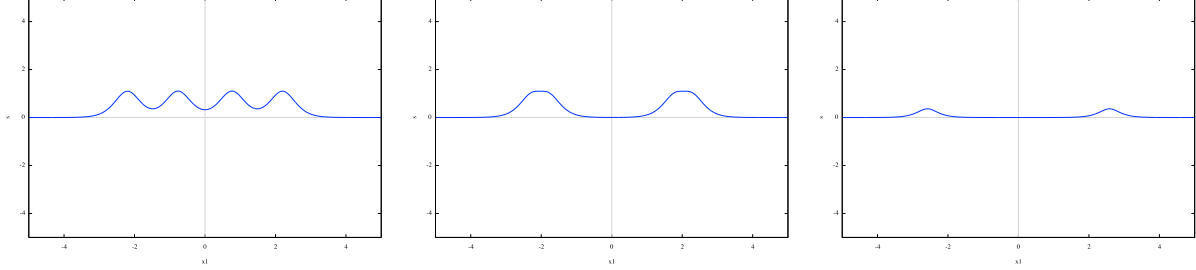


FIG. 31: For Eq. 58, action densities for $\delta = 5 \times 10^4$ (left), 5×10^5 (middle), 5×10^6 (right) with $\theta' = \pi/2$ fixed are depicted for $l_1 = 1, l_2 = 100$.

E. Combined effects of deformation parameters

The final step of analyzing the (global) stability of the non-BPS exact solution is to consider the five relevant deformation parameters at the same time. As a most significant effect, we consider the case where the strong phase dependence of two-body forces become most visible. Let us consider the following modification of the non-BPS exact solution

$$\omega = \left(\frac{2l_1}{l_2} e^{-\frac{2\pi}{3}z} + l_1 l_2 e^{-\frac{2\pi}{3}(2z+\bar{z})}, \quad e^{i\theta} - \delta e^{-\frac{2\pi}{3}(z+\bar{z})} - l_1^2 e^{-\frac{4\pi}{3}(z+\bar{z})}, \quad -l_2 e^{-\frac{2\pi}{3}\bar{z}} - \frac{2l_1^2}{l_2} e^{-\frac{2\pi}{3}(z+2\bar{z})} \right), \quad (59)$$

with $\delta \geq 0$, $0 \leq \theta < 2\pi$. We have chosen the phase of the the second term of the second component as $-\delta e^{-\frac{2\pi}{3}(z+\bar{z})}$, so that the strong phase dependence of two-body forces in Eq. (12) of both bions can collaborate together to act as attractive forces when $\theta = \pi$.

We depict the total action as a function of the symmetric separation $R = \frac{3}{2\pi} \log \frac{l_2^3}{\delta}$ of the bions at both right and left sides with $\theta = \pi$ fixed in Fig. 32, and compare it to the sum of the total action of each individual left and right bion. Up to numerical errors, these two plots are consistent. It indicates that the configuration (59) is seen as almost two-bion configurations, and there is no interaction between the two bions.

We note that the bion parts have the attractive interaction. It means that, if we calculate their amplitudes by integrating moduli integrals, we find the imaginary ambiguities, which will be cancelled out combined with the perturbative calculations around the appropriate background.

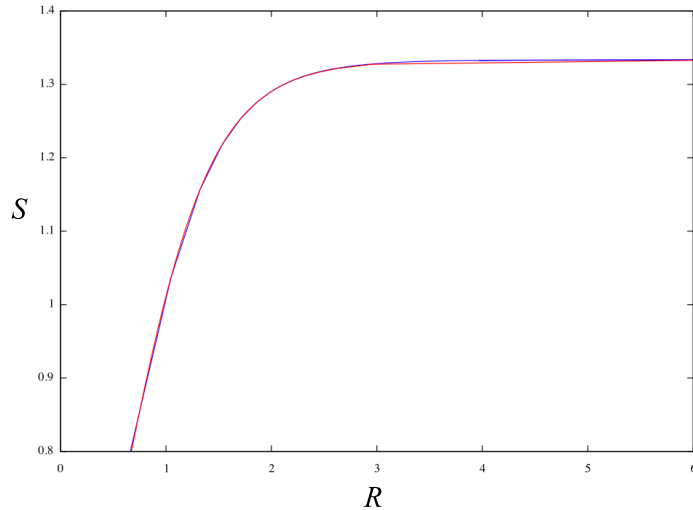


FIG. 32: The total action (red) as a function of the symmetric separation $R = \frac{3}{2\pi} \log \frac{l_2^3}{\delta}$ of the bions at both right and left sides Eq. (59). The results with $l_1 = 1, l_2 = 100, \theta = \pi$ (red) is compared with the sum of total actions of left and right bions (blue).

Again, we conclude that the non-BPS solutions can be seen as a special limit of the configurations relevant to the resurgence theory.

VI. NON-BPS SOLUTIONS IN GRASSMANN SIGMA MODELS

In this section, we briefly discuss extensions to the Grassmann sigma models $Gr_{N_F, N_C} \simeq SU(N)/SU(N_F - N_C) \times SU(N_C) \times U(1)$ with twisted boundary conditions. For this case, we have several ways of constructing non-BPS solutions [77, 78]. We introduce two simple classes of non-BPS solutions in the Grassmann sigma models.

A. Simple Extension of \mathbb{CP}^{N-1} Projection

We introduce one simple class of non-BPS solutions in the Grassmann model [77]. which is given by the following projection,

$$H_0^{\text{nonBPS}} = \begin{pmatrix} Z_+^{k_1} \omega \\ Z_+^{k_2} \omega \\ \cdot \\ \cdot \\ Z_+^{k_{N_c}} \omega \end{pmatrix}, \quad \omega \equiv \omega(z), \quad (60)$$

with

$$Z_+ : \omega \rightarrow Z_+ \omega \equiv \partial_z \omega - \frac{(\partial_z \omega) \omega^\dagger}{\omega \omega^\dagger} \omega, \quad (61)$$

and

$$0 \leq k_1 < k_2 < \dots < k_{N_c} \leq N_F - 1. \quad (62)$$

$\omega(z)$ is a arbitrary holomorphic N_F vector. This projection makes N_c N_F -vectors orthogonal. H_0 is a moduli matrix, which is related to the physical scalar H by $H = (H_0 H_0^\dagger)^{-1/2} H_0$ for this case since $H_0 H_0^\dagger$ is diagonal.

We apply this projection to $Gr_{4,2}$. We consider the holomorphic vector

$$\omega = \left(l_1 e^{i\theta_1} e^{-\pi z}, \quad l_2 e^{i\theta_2} e^{-\frac{\pi}{2} z}, \quad 1, \quad 0 \right). \quad (63)$$

It is nothing but the BPS solution of the \mathbb{CP}^3 model with $S = 1/2$, $Q = 1/2$. For example, we apply the projection with $k_1 = 0, k_2 = 1$ on the holomorphic vector ω , then one of non-BPS solutions in $Gr_{4,2}$ is given by

$$H_0^{\text{nonBPS}} = \begin{pmatrix} l_1 e^{-\pi z} & l_2 e^{-\frac{\pi}{2} z} & 1 & 0 \\ l_1 l_2^2 e^{-\frac{\pi}{2}(2z+\bar{z})} + 2l_1 e^{-\frac{\pi}{2} z} & -l_1^2 l_2 e^{-\pi(z+\bar{z})} + l_2 & -2l_1^2 e^{-\frac{\pi}{2}(z+2\bar{z})} - l_2^2 e^{-\frac{\pi}{2}\bar{z}} & 0 \end{pmatrix}. \quad (64)$$

We here drop the phase variables θ_1, θ_2 since they do not contribute to the action and topological charge densities. This solution is shown in Fig. 33. The total action of this solution is $S = 3/2$ while the total topological charge is $Q = 1/2$. It is notable that positions of constituent instantons in different color lines coincide in the configurations of the solution.

When we apply the projection with $k_1 = 1, k_2 = 2$ on the same holomorphic vector ω , we obtain a non-BPS solutions in $Gr_{4,2}$

$$H_0^{\text{nonBPS}} = \begin{pmatrix} l_1 l_2^2 e^{-\frac{\pi}{2}(2z+\bar{z})} + 2l_1 e^{-\frac{\pi}{2} z} & -l_1^2 l_2 e^{-\pi(z+\bar{z})} + l_2 & -2l_1^2 e^{-\frac{\pi}{2}(z+2\bar{z})} - l_2^2 e^{-\frac{\pi}{2}\bar{z}} & 0 \\ l_2 & 2l_1 e^{-\frac{\pi}{2}\bar{z}} & -l_1 l_2 e^{-\pi\bar{z}} & 0 \end{pmatrix}. \quad (65)$$

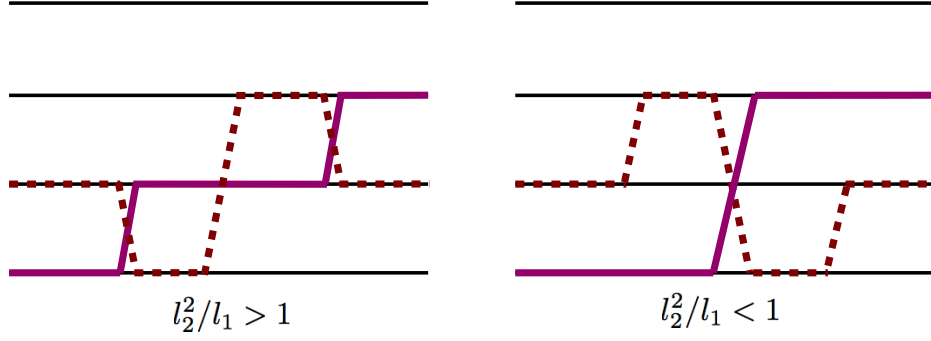


FIG. 33: The flipping partner configurations in the Non-BPS exact solution in $Gr_{4,2}$ model. Two different colored lines stand for two colors.

The total action of this solution is $S = 3/2$ while the total topological charge is $Q = -1/2$. This solution also has the transition between two seemingly distinct configurations in a similar way to the case of Fig. 33.

B. Projection Operation on Physical Scalars

As another class of non-BPS solutions, we introduce the class derived from the following projection on the physical scalar H^b for a BPS solution [77],

$$Z_+ : H^b \rightarrow Z_+ H^b \equiv \partial_z H^b - (\partial_z H^b)(H^b)^\dagger \left(H^b (H^b)^\dagger \right)^{-1} H^b. \quad (66)$$

Then, the scalar field H^{nonBPS} of the non-BPS solution from this projection is given as $H^{\text{nonBPS}} = (Z_+ H^b (Z_+ H^b)^\dagger)^{-1/2} Z_+ H^b$.

We here only concentrate on the simplest case, where the lines of different colors do not run on the same flavor vacua. We apply this projection to a BPS solution in $Gr_{6,2}$ with the moduli matrix

$$H_0^b = \begin{pmatrix} l_1 e^{i\theta_1} e^{-\frac{2\pi}{3}z} & l_2 e^{i\theta_2} e^{-\frac{\pi}{3}z} & 1 & 0 & 0 & 0 \\ 0 & 0 & 0 & l_3 e^{i\theta_3} e^{-\frac{2\pi}{3}z} & l_4 e^{i\theta_4} e^{-\frac{\pi}{3}z} & 1 \end{pmatrix} \quad (67)$$

with $S = 2/3$, $Q = 2/3$. The physical scalar H^b is derived as $H^b = (H_0^b (H_0^b)^\dagger)^{-1/2} H_0^b$ for this case. Then, the non-BPS solution derived from the above projection is

$$H^{\text{nonBPS}} = \begin{pmatrix} \frac{\omega^{(1)}}{|\omega^{(1)}|} & 0 & 0 & 0 \\ 0 & 0 & 0 & \frac{\omega^{(2)}}{|\omega^{(2)}|} \end{pmatrix}, \quad (68)$$

with

$$\omega^{(1)} = \left(l_1 l_2^2 e^{-\frac{\pi}{3}(2z+\bar{z})} + 2l_1 e^{-\frac{\pi}{3}z}, \quad -l_1^2 l_2 e^{-\frac{2\pi}{3}(z+\bar{z})} + l_2, \quad -2l_1^2 e^{-\frac{\pi}{3}(z+2\bar{z})} - l_2^2 e^{-\frac{\pi}{3}\bar{z}} \right), \quad (69)$$

and

$$\omega^{(2)} = \left(l_3 l_4^2 e^{-\frac{\pi}{3}(2z+\bar{z})} + 2l_3 e^{-\frac{\pi}{3}z}, \quad -l_3^2 l_4 e^{-\frac{2\pi}{3}(z+\bar{z})} + l_4, \quad -2l_3^2 e^{-\frac{\pi}{3}(z+2\bar{z})} - l_4^2 e^{-\frac{\pi}{3}\bar{z}} \right). \quad (70)$$

This solution is shown in Fig. 34 for $l_1 \ll l_2^2, l_3 \gg l_4^2$. The total action of this solution is $S = 4/3$ while the total topological charge is $Q = 0$.

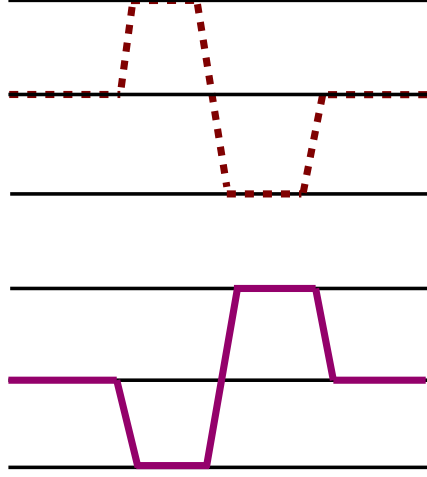


FIG. 34: A Non-BPS exact solution in $Gr_{6,2}$ model for $l_1 \ll l_2^2, l_3 \gg l_4^2$.

More generic forms of non-BPS solutions in Grassmann sigma model are discussed in [78]. We will discuss the properties of these non-BPS solutions and their relation to bions in Grassmann sigma model in the future works.

VII. SUMMARY AND DISCUSSION

We can summarize the present work as follows. Firstly, we have studied the non-BPS exact solutions in terms of ansatz for arbitrarily many fractional instantons, which gives solutions of field equations for asymptotically large separations of constituent fractional instantons. Since the ansatz serves as a basis to obtain all the multi-instanton contributions as integrals over the (quasi-)moduli, we find that the non-BPS exact solutions are also included as a part of multi-instanton contributions, which play an important role in the resurgence theory. Secondly, we have studied the balance of forces that assures the non-BPS configuration to be an exact solution. The interaction between a fractional instanton and a fractional anti-instanton is attractive (repulsive) depending on the value of the relative phase modulus θ . From this strong dependence of two-body forces, we found three essential properties of non-BPS exact solutions: (i) the appropriate relative sign in two

terms of the same component, (ii) the reflection symmetry around the middle compressed double fractional instanton, and (iii) the transition between two seemingly different configurations called flipping partners as moduli parameters vary. Thirdly, we have found a generic pattern of flipping partners that arises in the non-BPS exact solutions, and conjecture a diagrammatic procedure to find possible configurations in various other exact solutions. Fourthly, we have analyzed the local and global instabilities of the non-BPS exact solution in terms of the ansatz, and found the physical meaning of deformations that give negative modes and flow to other configurations of possible global saddle points. We have discussed the simple cases of non-BPS solutions in Grassmann sigma models based on Din-Zakrzewski projection method. The detailed study of properties of solutions will be a subject of future works.

The $U(N)$ Yang-Mills theory coupled with N Higgs fields in the fundamental representation admits a non-Abelian vortex solution, around which $\mathbb{C}P^{N-1}$ zero modes are localized [84–86]. BPS lump or instantons in the $\mathbb{C}P^{N-1}$ model on the vortex represent Yang-Mills instantons in the bulk point of view [73]. This correspondence was established in the BPS case. The non-BPS solutions in the $\mathbb{C}P^{N-1}$ model that we discussed should correspond to non-BPS solutions in the Yang-Mills theory. We can consider un-Higgsing by taking the decoupling limit of the Higgs fields. Then we may be able to obtain non-BPS multi-fractional-instanton or bion solutions in the Yang-Mills theory, that may shed light on the resurgence in the Yang-Mills theory.

Acknowledgments

We are grateful to Gerald Dunne for let the authors pay attention to the present subjects and thank the organizers for giving us a chance to discuss with him in “KEK Theory Workshop December 2015”. This work is supported in part by the Japan Society for the Promotion of Science (JSPS) Grant-in-Aid for Scientific Research (KAKENHI) Grant Numbers (16K17677 (T. M.), 25400268 (M. N.), 16H03984 (M. N.) and 25400241 (N. S.)). The work of M.N. is also supported in part by a Grant-in-Aid for Scientific Research on Innovative Areas “Topological Materials Science” (KAKENHI Grant No. 15H05855) and “Nuclear Matter in neutron Stars investigated by experiments and astronomical observations” (KAKENHI Grant No. 15H00841) from the Ministry of Education, Culture, Sports, Science, and Technology (MEXT) of Japan. This work is also supported by MEXT-Supported Program for the Strategic Research Foundation at Private

Universities “Topological Science” (Grant No. S1511006).

- [1] M. Ünsal, “Abelian duality, confinement, and chiral symmetry breaking in QCD(adj),” *Phys. Rev. Lett.* **100**, 032005 (2008) [arXiv:0708.1772 [hep-th]].
- [2] M. Ünsal, “Magnetic bion condensation: A New mechanism of confinement and mass gap in four dimensions,” *Phys. Rev. D* **80**, 065001 (2009) [arXiv:0709.3269 [hep-th]].
- [3] M. Shifman and M. Ünsal, “QCD-like Theories on $R(3) \times S(1)$: A Smooth Journey from Small to Large $r(S(1))$ with Double-Trace Deformations,” *Phys. Rev. D* **78**, 065004 (2008) [arXiv:0802.1232 [hep-th]].
- [4] E. Poppitz and M. Ünsal, “Conformality or confinement: (IR)relevance of topological excitations,” *JHEP* **0909**, 050 (2009) [arXiv:0906.5156 [hep-th]].
- [5] M. M. Anber and E. Poppitz, “Microscopic Structure of Magnetic Bions,” *JHEP* **1106**, 136 (2011) [arXiv:1105.0940 [hep-th]].
- [6] E. Poppitz, T. Schaefer and M. Ünsal, “Continuity, Deconfinement, and (Super) Yang-Mills Theory,” *JHEP* **1210**, 115 (2012) [arXiv:1205.0290 [hep-th]].
- [7] P. Argyres and M. Ünsal, “A semiclassical realization of infrared renormalons,” *Phys. Rev. Lett.* **109**, 121601 (2012) [arXiv:1204.1661 [hep-th]].
- [8] P. C. Argyres and M. Ünsal, “The semi-classical expansion and resurgence in gauge theories: new perturbative, instanton, bion, and renormalon effects,” *JHEP* **1208**, 063 (2012) [arXiv:1206.1890 [hep-th]].
- [9] G. V. Dunne and M. Ünsal, “Resurgence and Trans-series in Quantum Field Theory: The $CP(N-1)$ Model,” *JHEP* **1211**, 170 (2012) [arXiv:1210.2423 [hep-th]].
- [10] G. V. Dunne and M. Ünsal, “Continuity and Resurgence: towards a continuum definition of the $CP(N-1)$ model,” *Phys. Rev. D* **87**, 025015 (2013) [arXiv:1210.3646 [hep-th]].
- [11] R. Dabrowski and G. V. Dunne, “Fractionalized Non-Self-Dual Solutions in the $CP(N-1)$ Model,” *Phys. Rev. D* **88**, 025020 (2013) [arXiv:1306.0921 [hep-th]].
- [12] G. V. Dunne and M. Ünsal, “Generating Non-perturbative Physics from Perturbation Theory,” *Phys. Rev. D* **89**, 041701 (2014) [arXiv:1306.4405 [hep-th]].
- [13] A. Cherman, D. Dorigoni, G. V. Dunne and M. Ünsal, “Resurgence in QFT: Unitons, Fractons and Renormalons in the Principal Chiral Model,” *Phys. Rev. Lett.* **112**, 021601 (2014) [arXiv:1308.0127 [hep-th]].
- [14] G. Basar, G. V. Dunne and M. Ünsal, “Resurgence theory, ghost-instantons, and analytic continuation of path integrals,” *JHEP* **1310**, 041 (2013) [arXiv:1308.1108 [hep-th]].
- [15] G. V. Dunne and M. Ünsal, “Uniform WKB, Multi-instantons, and Resurgent Trans-Series,” *Phys. Rev. D* **89**, 105009 (2014) [arXiv:1401.5202 [hep-th]].
- [16] A. Cherman, D. Dorigoni and M. Ünsal, “Decoding perturbation theory using resurgence: Stokes

- phenomena, new saddle points and Lefschetz thimbles,” JHEP **1510**, 056 (2015) [arXiv:1403.1277 [hep-th]].
- [17] A. Behtash, T. Sulejmanpasic, T. Schafer and M. Unsal, “Hidden topological angles and Lefschetz thimbles,” Phys. Rev. Lett. **115**, no. 4, 041601 (2015) [arXiv:1502.06624 [hep-th]].
 - [18] S. Bolognesi and W. Zakrzewski, “Clustering and decomposition for non BPS solutions of the \mathbb{CP}^{N-1} models,” Phys. Rev. D **89**, 065013 (2014) [arXiv:1310.8247 [hep-th]].
 - [19] T. Misumi, M. Nitta and N. Sakai, “Neutral bions in the \mathbb{CP}^{N-1} model,” JHEP **1406**, 164 (2014) [arXiv:1404.7225 [hep-th]].
 - [20] T. Misumi, M. Nitta and N. Sakai, “Neutral bions in the \mathbb{CP}^{N-1} model for resurgence,” J. Phys. Conf. Ser. **597**, no. 1, 012060 (2015) [arXiv:1412.0861 [hep-th]].
 - [21] T. Misumi, M. Nitta and N. Sakai, “Resurgence in sine-Gordon quantum mechanics: Exact agreement between multi-instantons and uniform WKB,” JHEP **1509**, 157 (2015) [arXiv:1507.00408 [hep-th]].
 - [22] S. Shermer, “Twisted CP(N-1) instanton projectors and the N-level quantum density matrix,” arXiv:1412.3185 [hep-th].
 - [23] T. Misumi and T. Kanazawa, “Adjoint QCD on $\mathbb{R}^3 \times S^1$ with twisted fermionic boundary conditions,” JHEP **1406**, 181 (2014) [arXiv:1405.3113 [hep-ph]].
 - [24] T. Misumi, M. Nitta and N. Sakai, “Classifying bions in Grassmann sigma models and non-Abelian gauge theories by D-branes,” PTEP **2015**, 033B02 (2015) [arXiv:1409.3444 [hep-th]].
 - [25] M. Nitta, “Fractional instantons and bions in the $O(N)$ model with twisted boundary conditions,” JHEP **1503**, 108 (2015) [arXiv:1412.7681 [hep-th]].
 - [26] M. Nitta, “Fractional instantons and bions in the principal chiral model on $\mathbb{R}^2 \times S^1$ with twisted boundary conditions,” JHEP **1508**, 063 (2015) [arXiv:1503.06336 [hep-th]].
 - [27] G. V. Dunne and M. Unsal, “Resurgence and Dynamics of $O(N)$ and Grassmannian Sigma Models,” JHEP **1509**, 199 (2015) [arXiv:1505.07803 [hep-th]].
 - [28] A. Behtash, E. Poppitz, T. Sulejmanpasic and M. Unsal, “The curious incident of multi-instantons and the necessity of Lefschetz thimbles,” JHEP **1511**, 175 (2015) [arXiv:1507.04063 [hep-th]].
 - [29] A. Behtash, G. V. Dunne, T. Schafer, T. Sulejmanpasic and M. Unsal, “Complexified path integrals, exact saddles and supersymmetry,” Phys. Rev. Lett. **116**, no. 1, 011601 (2016) [arXiv:1510.00978 [hep-th]].
 - [30] A. Behtash, G. V. Dunne, T. Schaefer, T. Sulejmanpasic and M. Unsal, “Toward Picard-Lefschetz Theory of Path Integrals, Complex Saddles and Resurgence,” arXiv:1510.03435 [hep-th].
 - [31] G. V. Dunne and M. Unsal, “What is QFT? Resurgent trans-series, Lefschetz thimbles, and new exact saddles,” arXiv:1511.05977 [hep-lat].
 - [32] I. Gahramanov and K. Tezgin, “A remark on the Dunne-Unsal relation in exact semi-classics,” Phys. Rev. D **93**, no. 6, 065037 (2016) [arXiv:1512.08466 [hep-th]].
 - [33] G. V. Dunne and M. Unsal, “New Methods in QFT and QCD: From Large-N Orbifold Equivalence to Bions and Resurgence,” arXiv:1601.03414 [hep-th].

- [34] G. V. Dunne and M. Unsal, “WKB and Resurgence in the Mathieu Equation,” arXiv:1603.04924 [math-ph].
- [35] G. 't Hooft, “Can We Make Sense Out of Quantum Chromodynamics?,” Subnucl. Ser. **15**, 943 (1979).
- [36] V. A. Fateev, V. A. Kazakov and P. B. Wiegmann, “Principal chiral field at large N ,” Nucl. Phys. B **424**, 505 (1994) [hep-th/9403099].
- [37] V. A. Fateev, P. B. Wiegmann and V. A. Kazakov, “Large N chiral field in two-dimensions,” Phys. Rev. Lett. **73**, 1750 (1994).
- [38] J. Ecalle, “Les Fonctions Resurgentes”, Vol. I - III (Publ. Math. Orsay, 1981).
- [39] M. Marino, R. Schiappa and M. Weiss, “Nonperturbative Effects and the Large-Order Behavior of Matrix Models and Topological Strings,” Commun. Num. Theor. Phys. **2**, 349 (2008) [arXiv:0711.1954 [hep-th]].
- [40] M. Marino, “Nonperturbative effects and nonperturbative definitions in matrix models and topological strings,” JHEP **0812**, 114 (2008) [arXiv:0805.3033 [hep-th]].
- [41] M. Marino, R. Schiappa and M. Weiss, “Multi-Instantons and Multi-Cuts,” J. Math. Phys. **50**, 052301 (2009) [arXiv:0809.2619 [hep-th]].
- [42] S. Pasquetti and R. Schiappa, “Borel and Stokes Nonperturbative Phenomena in Topological String Theory and $c=1$ Matrix Models,” Annales Henri Poincare **11**, 351 (2010) [arXiv:0907.4082 [hep-th]].
- [43] N. Drukker, M. Marino and P. Putrov, “From weak to strong coupling in ABJM theory,” Commun. Math. Phys. **306**, 511 (2011) [arXiv:1007.3837 [hep-th]].
- [44] I. Aniceto, R. Schiappa and M. Vonk, “The Resurgence of Instantons in String Theory,” Commun. Num. Theor. Phys. **6**, 339 (2012) [arXiv:1106.5922 [hep-th]].
- [45] M. Marino, “Lectures on non-perturbative effects in large N gauge theories, matrix models and strings,” Fortsch. Phys. **62**, 455 (2014) [arXiv:1206.6272 [hep-th]].
- [46] Y. Hatsuda, S. Moriyama and K. Okuyama, “Instanton Bound States in ABJM Theory,” JHEP **1305**, 054 (2013) [arXiv:1301.5184 [hep-th]].
- [47] R. Schiappa and R. Vaz, “The Resurgence of Instantons: Multi-Cut Stokes Phases and the Painleve II Equation,” Commun. Math. Phys. **330**, 655 (2014) [arXiv:1302.5138 [hep-th]].
- [48] Y. Hatsuda, M. Marino, S. Moriyama and K. Okuyama, “Non-perturbative effects and the refined topological string,” JHEP **1409**, 168 (2014) [arXiv:1306.1734 [hep-th]].
- [49] I. Aniceto and R. Schiappa, “Nonperturbative Ambiguities and the Reality of Resurgent Transseries,” Commun. Math. Phys. **335**, no. 1, 183 (2015) [arXiv:1308.1115 [hep-th]].
- [50] R. Couso-Santamaria, J. D. Edelstein, R. Schiappa and M. Vonk, “Resurgent Transseries and the Holomorphic Anomaly,” Annales Henri Poincare **17**, no. 2, 331 (2016) [arXiv:1308.1695 [hep-th]].
- [51] J. Kallen and M. Marino, “Instanton effects and quantum spectral curves,” arXiv:1308.6485 [hep-th].
- [52] M. Honda and S. Moriyama, “Instanton Effects in Orbifold ABJM Theory,” JHEP **1408**, 091 (2014) [arXiv:1404.0676 [hep-th]].
- [53] A. Grassi, M. Marino and S. Zakany, “Resumming the string perturbation series,” JHEP **1505**, 038

- (2015) [arXiv:1405.4214 [hep-th]].
- [54] D. Sauzin, “Introduction to 1-summability and resurgence,” arXiv:1405.0356 [math.DS].
 - [55] J. Kallen, “The spectral problem of the ABJ Fermi gas,” arXiv:1407.0625 [hep-th].
 - [56] R. Couso-Santamaria, J. D. Edelstein, R. Schiappa and M. Vonk, “Resurgent Transseries and the Holomorphic Anomaly: Nonperturbative Closed Strings in Local \mathbb{CP}^2 ,” Commun. Math. Phys. **338**, no. 1, 285 (2015) [arXiv:1407.4821 [hep-th]].
 - [57] M. Honda, “On Perturbation theory improved by Strong coupling expansion,” JHEP **1412**, 019 (2014) [arXiv:1408.2960 [hep-th]].
 - [58] I. Aniceto, J. G. Russo and R. Schiappa, “Resurgent Analysis of Localizable Observables in Supersymmetric Gauge Theories,” JHEP **1503**, 172 (2015) [arXiv:1410.5834 [hep-th]].
 - [59] R. Couso-Santamaria, R. Schiappa and R. Vaz, “Finite N from Resurgent Large N,” Annals Phys. **356**, 1 (2015) [arXiv:1501.01007 [hep-th]].
 - [60] M. Honda and D. P. Jatkar, Nucl. Phys. B **900**, 533 (2015) [arXiv:1504.02276 [hep-th]].
 - [61] Y. Hatsuda and K. Okuyama, “Resummations and Non-Perturbative Corrections,” JHEP **1509**, 051 (2015) [arXiv:1505.07460 [hep-th]].
 - [62] I. Aniceto, “The Resurgence of the Cusp Anomalous Dimension,” J. Phys. A **49**, 065403 (2016) [arXiv:1506.03388 [hep-th]].
 - [63] D. Dorigoni and Y. Hatsuda, “Resurgence of the Cusp Anomalous Dimension,” JHEP **1509**, 138 (2015) [arXiv:1506.03763 [hep-th]].
 - [64] M. Honda, “Borel summability of perturbative series in 4d N=2 and 5d N=1 theories,” arXiv:1603.06207 [hep-th].
 - [65] E. B. Bogomolny, “Calculation Of Instanton - Anti-instanton Contributions In Quantum Mechanics,” Phys. Lett. B **91**, 431 (1980).
 - [66] J. Zinn-Justin, “Multi - Instanton Contributions in Quantum Mechanics,” Nucl. Phys. B **192**, 125 (1981).
 - [67] J. Zinn-Justin, “Multi - Instanton Contributions in Quantum Mechanics. 2.,” Nucl. Phys. B **218** (1983) 333.
 - [68] J. Zinn-Justin, “Instantons in Quantum Mechanics: Numerical Evidence for a Conjecture,” J. Math. Phys. **25** (1984) 549.
 - [69] J. Zinn-Justin and U. D. Jentschura, “Multi-instantons and exact results I: Conjectures, WKB expansions, and instanton interactions,” Annals Phys. **313**, 197 (2004) [quant-ph/0501136].
 - [70] J. Zinn-Justin and U. D. Jentschura, “Multi-instantons and exact results II: Specific cases, higher-order effects, and numerical calculations,” Annals Phys. **313**, 269 (2004) [quant-ph/0501137].
 - [71] U. D. Jentschura, A. Surzhykov and J. Zinn-Justin, “Multi-instantons and exact results. III: Unification of even and odd anharmonic oscillators,” Annals Phys. **325**, 1135 (2010).
 - [72] U. D. Jentschura and J. Zinn-Justin, “Multi-instantons and exact results. IV: Path integral formalism,” Annals Phys. **326**, 2186 (2011).

- [73] M. Eto, Y. Isozumi, M. Nitta, K. Ohashi and N. Sakai, “Instantons in the Higgs phase,” *Phys. Rev. D* **72**, 025011 (2005) [hep-th/0412048].
- [74] M. Eto, T. Fujimori, Y. Isozumi, M. Nitta, K. Ohashi, K. Ohta and N. Sakai, “Non-Abelian vortices on cylinder: Duality between vortices and walls,” *Phys. Rev. D* **73**, 085008 (2006) [hep-th/0601181]; M. Eto, T. Fujimori, M. Nitta, K. Ohashi, K. Ohta and N. Sakai, “Statistical mechanics of vortices from D-branes and T-duality,” *Nucl. Phys. B* **788**, 120 (2008) [hep-th/0703197].
- [75] F. Bruckmann, “Instanton constituents in the $O(3)$ model at finite temperature,” *Phys. Rev. Lett.* **100**, 051602 (2008) [arXiv:0707.0775 [hep-th]]; W. Brendel, F. Bruckmann, L. Janssen, A. Wipf and C. Wozar, “Instanton constituents and fermionic zero modes in twisted CP^{n-1} models,” *Phys. Lett. B* **676**, 116 (2009) [arXiv:0902.2328 [hep-th]]; D. Harland, “Kinks, chains, and loop groups in the CP^{n-1} sigma models,” *J. Math. Phys.* **50**, 122902 (2009) [arXiv:0902.2303 [hep-th]]; F. Bruckmann and T. Sulejmanpasic, “Nonlinear sigma models at nonzero chemical potential: breaking up instantons and the phase diagram,” *Phys. Rev. D* **90**, no. 10, 105010 (2014) [arXiv:1408.2229 [hep-th]].
- [76] A. M. Din and W. J. Zakrzewski, “General Classical Solutions in the $CP^{(n-1)}$ Model,” *Nucl. Phys. B* **174**, 397 (1980); “Interpretation and Further Properties of General Classical $CP^{(n-1)}$ Solutions,” *Nucl. Phys. B* **182**, 151 (1981); W. J. Zakrzewski, *Low Dimensional Sigma Models*, (Taylor and Francis, 1989).
- [77] A. M. Din and W. J. Zakrzewski, “Classical Solutions in Grassmannian σ Models,” *Lett. Math. Phys.* **5**, 553 (1981).
- [78] A. M. Din and W. J. Zakrzewski, “Some Properties Of Classical Solutions In Grassmannian Sigma Models,” *Lett. Math. Phys.* **7**, 505 (1983).
- [79] M. Eto, Y. Isozumi, M. Nitta, K. Ohashi and N. Sakai, “Solitons in the Higgs phase: The Moduli matrix approach,” *J. Phys. A* **39**, R315 (2006) [hep-th/0602170].
- [80] M. Eto, Y. Isozumi, M. Nitta, K. Ohashi, K. Ohta and N. Sakai, “D-brane construction for non-Abelian walls,” *Phys. Rev. D* **71**, 125006 (2005) [hep-th/0412024].
- [81] Y. Isozumi, M. Nitta, K. Ohashi and N. Sakai, “Construction of non-Abelian walls and their complete moduli space,” *Phys. Rev. Lett.* **93**, 161601 (2004) [hep-th/0404198].
- [82] Y. Isozumi, M. Nitta, K. Ohashi and N. Sakai, “Non-Abelian walls in supersymmetric gauge theories,” *Phys. Rev. D* **70**, 125014 (2004) [hep-th/0405194].
- [83] D. Tong, “The Moduli space of BPS domain walls,” *Phys. Rev. D* **66**, 025013 (2002) [hep-th/0202012].
- [84] A. Hanany and D. Tong, “Vortices, instantons and branes,” *JHEP* **0307**, 037 (2003) [hep-th/0306150].
- [85] R. Auzzi, S. Bolognesi, J. Evslin, K. Konishi and A. Yung, “NonAbelian superconductors: Vortices and confinement in $N=2$ SQCD,” *Nucl. Phys. B* **673**, 187 (2003) [hep-th/0307287].
- [86] M. Eto, Y. Isozumi, M. Nitta, K. Ohashi and N. Sakai, “Moduli space of non-Abelian vortices,” *Phys. Rev. Lett.* **96**, 161601 (2006) [hep-th/0511088].
- [87] If $N = 2$, the upper and lower lines are identified in Fig. 3 (b) (and (c)), and the corresponding ansatz becomes more complicated, since it involves an (anti-)instanton with $|Q| = 1$ in the middle.